Cosmogenic ^{10}Be and ^{36}Cl geochronology of offset alluvial fans along the northern Death Valley fault zone: Implications for transient strain in the eastern California shear zone

Kurt L. Frankel,[1] Katherine S. Brantley,[2] James F. Dolan,[1] Robert C. Finkel,[3] Ralph E. Klinger,[4] Jeffrey R. Knott,[5] Michael N. Machette,[6] Lewis A. Owen,[7] Fred M. Phillips,[8] Janet L. Slate,[6] and Brian P. Wernicke[2]

Received 15 February 2006; revised 16 January 2007; accepted 30 January 2007; published 13 June 2007.

[1] The northern Death Valley fault zone (NDVFZ) has long been recognized as a major right-lateral strike-slip fault in the eastern California shear zone (ECSZ). However, its geologic slip rate has been difficult to determine. Using high-resolution digital topographic imagery and terrestrial cosmogenic nuclide dating, we present the first geochronologically determined slip rate for the NDVFZ. Our study focuses on the Red Wall Canyon alluvial fan, which exposes clean dextral offsets of seven channels. Analysis of airborne laser swath mapping data indicates ~297 ± 9 m of right-lateral displacement on the fault system since the late Pleistocene. In situ terrestrial cosmogenic ^{10}Be and ^{36}Cl geochronology was used to date the Red Wall Canyon fan and a second, correlative fan also cut by the fault. Beryllium 10 dates from large cobbles and boulders provide a maximum age of 70 +22/−20 ka for the offset landforms. The minimum age of the alluvial fan deposits based on ^{36}Cl depth profiles is 63 ± 8 ka. Combining the offset measurement with the cosmogenic ^{10}Be date yields a geologic fault slip rate of 4.2 +1.9/−1.1 mm yr^{-1}, whereas the ^{36}Cl data indicate 4.7 +0.9/−0.6 mm yr^{-1} of slip. Summing these slip rates with known rates on the Owens Valley, Hunter Mountain, and Stateline faults at similar latitudes suggests a total geologic slip rate across the northern ECSZ of ~8.5 to 10 mm yr^{-1}. This rate is commensurate with the overall geodetic rate and implies that the apparent discrepancy between geologic and geodetic data observed in the Mojave section of the ECSZ does not extend north of the Garlock fault. Although the overall geodetic rates are similar, the best estimates based on geology predict higher strain rates in the eastern part of the ECSZ than to the west, whereas the observed geodetic strain is relatively constant.

Citation: Frankel, K. L., et al. (2007), Cosmogenic ^{10}Be and ^{36}Cl geochronology of offset alluvial fans along the northern Death Valley fault zone: Implications for transient strain in the eastern California shear zone, *J. Geophys. Res.*, *112*, B06407, doi:10.1029/2006JB004350.

1. Introduction

[2] Whether strain storage and release rates are constant or nonuniform over geologic time is a fundamental, unresolved issue in modern geodynamics. Comparisons of short-term (decadal) geodetic data with long-term (thousand to million year) geologic data indicate that strain storage and release rates are comparable along most plate boundaries [*Sella et al.*, 2002]. Along the Pacific–North American plate boundary, where plate motion is partitioned between the San Andreas fault and relatively low strain rate, intraplate faults of the eastern California shear zone (ECSZ) and Basin and Range [e.g., *Bennett et al.*, 2003], recent comparisons of geodetic and geologic strain rates reveal significant discrepancies. The Mojave section of the ECSZ south of the Garlock fault exhibits a pronounced strain transient [*Peltzer et al.*, 2001; *Oskin and Iriondo*, 2004] wherein the geodetic rates appear to be as much as twice the longer-term geologic

[1]Department of Earth Sciences, University of Southern California, Los Angeles, California, USA.
[2]Division of Geological and Planetary Sciences, California Institute of Technology, Pasadena, California, USA.
[3]Center for Accelerator Mass Spectrometry, Lawrence Livermore National Laboratory, Livermore, California, USA.
[4]Technical Service Center, U.S. Bureau of Reclamation, Denver, Colorado, USA.
[5]Department of Geological Sciences, California State University, Fullerton, California, USA.
[6]Central Region Geologic Hazards Team, U.S. Geological Survey, Lakewood, Colorado, USA.
[7]Department of Geology, University of Cincinnati, Cincinnati, Ohio, USA.
[8]Department of Earth and Environmental Science, New Mexico Institute of Mining and Technology, Socorro, New Mexico, USA.

0148-0227/07/2006JB004350$09.00

rates [*Dixon et al.*, 2000; *McClusky et al.*, 2001; *Peltzer et al.*, 2001; *Oskin and Iriondo*, 2004; *Oskin et al.*, 2006, 2007]. Similarly, along the eastern margin of the ECSZ north of the Garlock fault, geodetic right-lateral shear of $\sim$1.2 mm yr^{-1} across the Yucca Mountain area is not accommodated by any comparable Quaternary structure [*Wernicke et al.*, 2004; *Friedrich et al.*, 2004].

[3] These observations raise several fundamentally important questions about how strain accumulates and is released along major plate boundary fault systems. Most basically, how temporally constant are strain accumulation and release? Are geologic slip rates averaged over thousands to millions of years compatible with short-term geodetic rates, or do strain transients commonly occur? If transients do occur, over what timescales do they operate? Are strain transients localized features tied to regions of structural complexity or are they more fundamental features of plate boundary motion [e.g., *Dixon et al.*, 2003; *Friedrich et al.*, 2003; *Bennett et al.*, 2004; *Wernicke et al.*, 2005; *Dolan et al.*, 2007]?

[4] In this paper, we address these questions as they pertain to the Pacific–North America plate boundary by determining a long-term geologic slip rate on the northern Death Valley fault zone (NDVFZ; Figure 1). Acquisition of high-resolution airborne laser swath mapping (ALSM; also known as lidar) digital topographic data allows us to restore deformed alluvial landforms in unprecedented detail along the trace of the fault. In the past it was difficult to quantitatively determine the precise age of Pleistocene deposits in arid environments due to the lack of datable materials. Over the past two decades, however, the advent of terrestrial cosmogenic nuclide geochronology has allowed researchers to resolve numerical ages for a variety of depositional landforms [*Phillips et al.*, 1986; *Lal*, 1987; *Elmore and Phillips*, 1987; *Finkel and Suter*, 1993; *Bierman et al.*, 1995; *Anderson et al.*, 1996; *Hancock et al.*, 1999; *Gosse and Phillips*, 2001; *van der Woerd et al.*, 2002; *Matmon et al.*, 2005, 2006; *van der Woerd et al.*, 2006]. Dating offset landforms along the NDVFZ by in situ terrestrial cosmogenic ^{10}Be and ^{36}Cl, two independent, yet complementary techniques, yields a more precise geologic slip rate on the NDVFZ and provides the first direct comparison between the two geochronometers from the same deposit. The slip rates presented here fill in a major missing piece of the strain "puzzle" in the ECSZ.

2. Active Tectonics of the Eastern California Shear Zone

2.1. Eastern California Shear Zone

[5] The ECSZ and its northern equivalent, the Walker Lane belt of western Nevada, extend more than 800 km north from the eastern Transverse Ranges in southern California, through the Mojave Desert and along the westernmost portion of the Basin and Range province (Figure 1). The ECSZ is characterized by a system of predominantly right-lateral, strike-slip faults and normal faults that accommodate $\sim$20–25% of the total relative motion between the Pacific and North America plates [*Dokka and Travis*, 1990; *Humphreys and Weldon*, 1994; *Bennett et al.*, 1997; *Reheis and Sawyer*, 1997; *McClusky et al.*, 2001; *Bennett et al.*, 2003; *Dixon et al.*, 2003].

[6] In the Mojave Desert, south of the left-lateral Garlock fault, the southern ECSZ comprises a $\sim$100-km-wide network of north-northwest trending right-lateral faults. Geodetic data indicate that elastic strain is accumulating across this zone at 12 ± 2 mm yr^{-1} [*Savage et al.*, 1990; *Bennett et al.*, 1997; *Gan et al.*, 2000; *McClusky et al.*, 2001; *Miller et al.*, 2001; *Peltzer et al.*, 2001]. Both seismological and paleoseismological data indicate that the southern ECSZ is releasing strain at a relatively rapid rate. Specifically, portions of several of the faults in this region ruptured during the 1992 M_w 7.3 Landers and 1999 M_w 7.1 Hector Mine earthquakes (Figure 1). Furthermore, paleoseismologic data indicate that these two earthquakes are part of an ongoing, $\geq$1000-year-long seismic cluster [*Rockwell et al.*, 2000]. However, such evidence for rapid strain accumulation and release during the recent past is at odds with geologic slip rate data. The long-term, cumulative slip rate across the Mojave segment of the ECSZ is much slower (by about half) than the current rate of strain accumulation [*Oskin et al.*, 2006, 2007]. These observations suggest the occurrence of a pronounced strain transient across the southern ECSZ.

[7] Displacement from the southern ECSZ continues north across the Garlock fault into the northern ECSZ, which consists of four major fault systems: the Owens Valley (OVFZ), Panamint Valley–Saline Valley–Hunter Mountain (HMFZ), northern Death Valley, and Stateline (SLFZ) fault zones (Figures 1 and 2). Farther north, most of the dextral motion between the Sierra Nevada block and North America is focused on the White Mountains and Fish Lake Valley fault zones bounding the east and west sides of the White Mountains, respectively (Figure 2) [*Dixon et al.*, 2000]. In addition to the major north trending dextral faults, a number of northeast trending faults transfer slip between faults of the Owens and Panamint Valley fault systems and the Death Valley fault system (Figure 2) [*Dixon et al.*, 1995; *Reheis and Dixon*, 1996]. These predominantly down-to-the-northwest extensional faults include the Deep Springs, Towne Pass, and Tin Mountain faults [*Dixon et al.*, 1995; *Lee et al.*, 2001a; *Klinger*, 2001]. For detailed descriptions of individual faults in the northern ECSZ, please see the auxiliary materials[1].

2.2. Death Valley Fault System

[8] The $\sim$310-km-long Death Valley fault system, which includes the Fish Lake Valley fault zone [*Reheis and Sawyer*, 1997; *Machette et al.*, 2001], is the largest and most continuous fault system in the ECSZ (Figure 1). The NDVFZ transitions into the Fish Lake Valley fault zone to the north (Figure 2) [*Machette et al.*, 2001]. Both of these faults offset Quaternary deposits. In contrast, the southeastern extent of the NDVFZ, the Furnace Creek fault zone, does not offset Quaternary deposits in southernmost Amargosa Valley [*Machette et al.*, 2001]. Net offset of pre-11.6 ± 0.3 Ma [*Niemi et al.*, 2001] markers found in both the Cottonwood and Funeral Mountains is 68 ± 4 km [*Snow and Wernicke*, 1989]. This yields an average post-mid-Miocene slip rate of 5.9 ± 0.4 mm yr^{-1} for the combined traces of the northern Death Valley and Furnace Creek fault zones.

[1] Auxiliary material data sets are available at ftp://ftp.agu.org/apend/jb/2006jb004350. Other auxiliary material files are in the HTML.

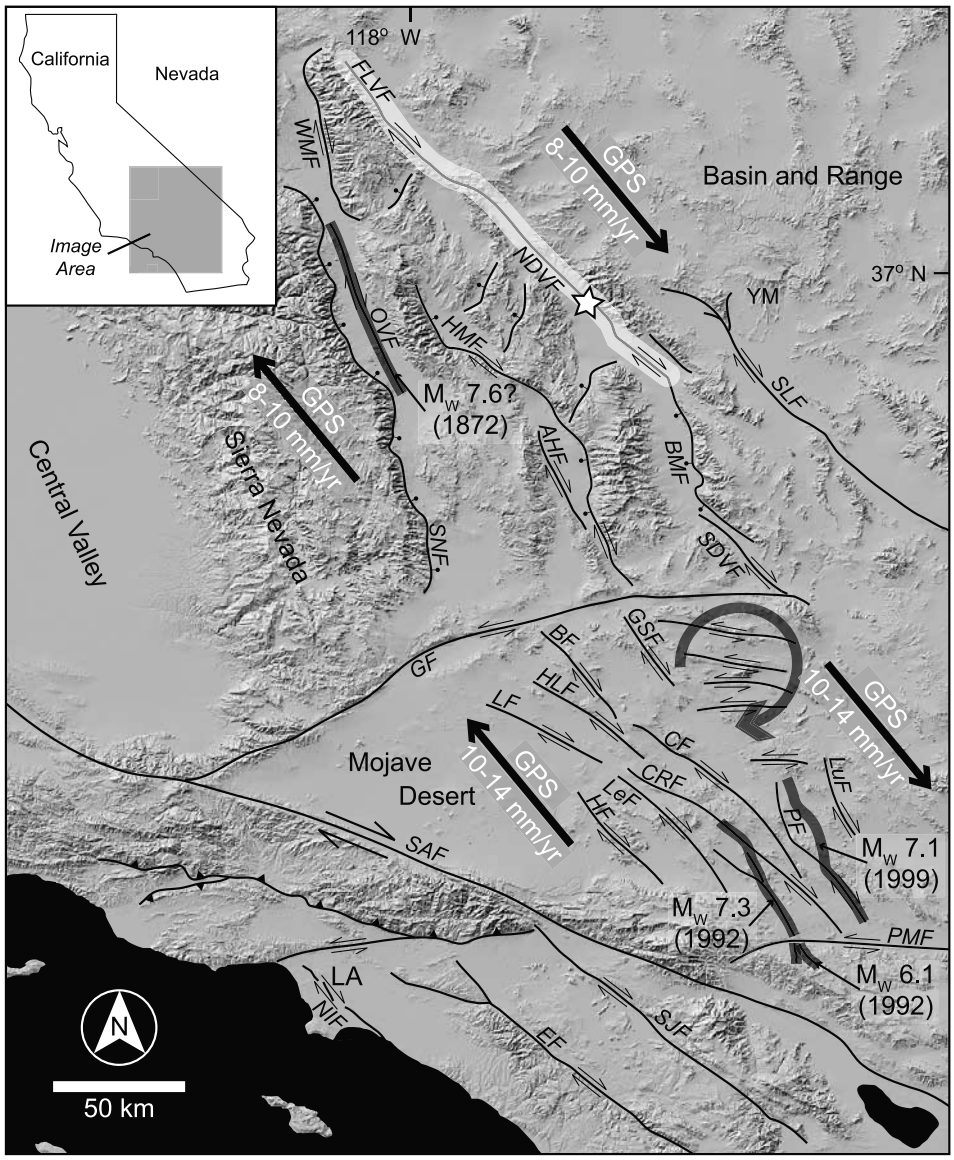

Figure 1. Index map of the eastern California shear zone (ECSZ). The Death Valley and Fish Lake Valley fault zones are highlighted in white. Recent, major ECSZ surface ruptures are shown in dark gray. The white star indicates the location of the Red Wall Canyon and Big Dip Canyon alluvial fans. FLVF, Fish Lake Valley fault zone; WMF, White Mountains fault zone; NDVF, northern Death Valley fault zone; BMF, Black Mountains fault zone; HMF, Hunter Mountain–Saline Valley fault zone; OVF, Owens Valley fault; SDVF, Southern Death Valley fault; SLF, Stateline fault zone; SNF, Sierra Nevada frontal fault; AHF, Ash Hill fault; GF, Garlock fault; LF, Lockhart fault; HLF, Harper Lake fault; BF, Blackwater fault; GSF, Goldstone fault; HF, Helendale fault; LeF, Len wood fault; CRF, Camp Rock fault; CF, Calico fault; PF, Pisgah fault; LuF, Ludlow fault; PMF, Pinto Mountain fault; SAF, San Andreas fault; NIF, Newport-Inglewood fault; EF, Elsinore fault; SJF, San Jacinto fault; LA, Los Angeles; and YM, Yucca Mountain. Geodetic (GPS) rates are from *Savage et al.* [1990], *Dixon et al.* [1995], *Gan et al.* [2000], and *Bennett et al.* [2003].

[9] Both geologic and geodetic observations suggest that the northern Death Valley and Fish Lake Valley fault zones accommodate the majority of slip in the ECSZ north of the Garlock fault. Estimates of the slip rate for the NDVFZ based on geodetic data range from ~3 to 8 mm yr^{-1} [*Savage et al.*, 1990; *Humphreys and Weldon*, 1994; *Bennett et al.*, 1997; *Dixon et al.*, 2000; *McClusky et al.*, 2001; *Dixon et al.*, 2003; *Bennett et al.*, 2003]. The total contemporary displacement rate between the central Panamint Range (GPS site ROGE, which is ~20 km WSW of the Death Valley fault system and an equal distance ENE of the Panamint Valley fault system) and the relatively stable central Great Basin region is 3.6 ± 0.2 mm yr^{-1} [*Wernicke et al.*, 2005]. Because a significant fraction of ROGE's

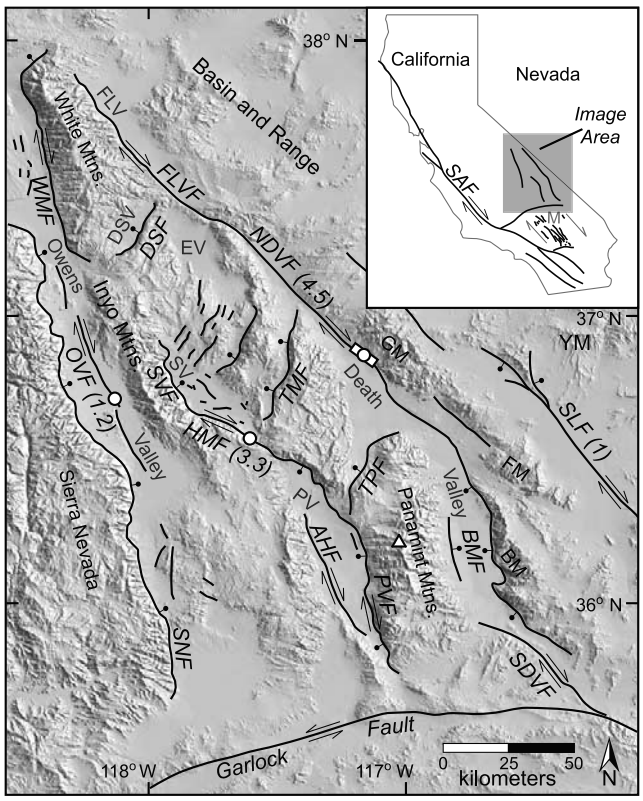

Figure 2. Detailed index map of the northern part of the eastern California shear zone showing the relationship between the Owens Valley, Hunter Mountain, northern Death Valley, and Stateline fault zones. The white box on the northern Death Valley fault zone indicates the location of Figure 5. White triangle shows the location of GPS site ROGE. Numbers in parentheses next to fault names indicate the preferred long-term slip rate of the fault, and white circles represent locations where the slip rate was determined. Slip rates are from this study, *Lee et al.* [2001b], *Oswald and Wesnousky* [2002], and *Schweickert and Lahren* [1997]. See text for discussion. WMF, White Mountains fault zone; FLV, Fish Lake Valley; FLVF, Fish Lake Valley fault zone; DSV, Deep Springs Valley; EV, Eureka Valley; NDVF, northern Death Valley fault zone; SDVF, southern Death Valley fault zone; BMF, Black Mountains fault zone; SV, Saline Valley; SVF, Saline Valley fault zone; OVF, Owens Valley fault zone; HMF, Hunter Mountain fault zone, SLF, Stateline fault zone; PV, Panamint Valley; AHF, Ash Hill fault; PVF, Panamint Valley fault zone; GM, Grapevine Mountains; FM, Funeral Mountains; BM, Black Mountains; SNF, Sierra Nevada frontal fault; DSF, Deep Springs fault; TMF, Tin Mountain fault; TPF, Towne Pass fault, and YM, Yucca Mountain.

motion may be attributable to the Panamint Valley fault system as well as the SLFZ, this rate should be considered a firm upper bound on the contemporary geodetic displacement along the NDVFZ. The best estimate of total motion across the ECSZ/Walker Lane belt, including continuous GPS data, is 9.3 ± 0.2 mm yr^{-1} [*Bennett et al.*, 2003]. This estimate is relatively low compared with previous, less robust estimates, but closer to a sum of estimated geologic slip rates on faults in the region.

[10] Studies estimating the 1000 year to 1,000,000 year geologic slip rates on the NDVFZ are sparse [*Brogan et al.*, 1991; *Reheis and Sawyer*, 1997; *Klinger*, 2001]. *Klinger* [2001] used tephrochronology and soil development to estimate Holocene to Pleistocene slip rates of 3 to 9 mm yr^{-1} on the NDVFZ. The broad range of slip rates highlights the difficulties associated with obtaining age control. Soil geomorphic ages are semiquantitative and provide a reasonable correlative age, but they are not equivalent to geochronology. Tephrochronology is generally accurate and precise, but in Death Valley, the large number of nearby Long Valley caldera eruptions often makes correlations tentative [*Klinger*, 2001]. Although previous studies suggest slip rates that are broadly in agreement with geodetic estimates, improving upon them through direct dating of offset geomorphic features allows for a more robust comparison between geodetic and geologic rates. This study further refines the slip rate on this important fault by dating and restoring the dextral offset on the Red Wall Canyon alluvial fan in northern Death Valley.

3. Study Area

[11] The alluvial fans at the mouth of Red Wall and Big Dip Canyons, which drain the western flank of the Grapevine Mountains are offset by the NDVFZ (Figures 1 and 2). *Reynolds* [1969] estimated the offset of Red Wall Canyon stream channels at 46 m. *Klinger* [2001] mapped six alluvial units ranging in age from late Pleistocene to the active channels, and documented 250 to 330 m of dextral offset. At Big Dip Canyon, *Brogan et al.* [1991] mapped a shutter ridge along the west side of the NDVFZ that effectively isolates older alluvial fan deposits to the west.

[12] Alluvial fan deposits in Death Valley are consistent with the ubiquitous desert piedmont deposits (Q1, Q2, Q3, and Q4) that can be correlated throughout southwestern North America by geomorphic expression and soil development [*Bull*, 1991]. Regionally, the Q2 surface is generally considered late Pleistocene in age and was deposited in a semiarid environment during a slight warming in otherwise average glacial conditions during oxygen isotope stage four [*Bull*, 1991; M. N. Machette et al., Terrestrial cosmogenic-nuclide (TCN) ages for alluvial fans in Death Valley National Park, California, submitted to *Geological Society of America Bulletin*, 2007, hereinafter referred to as Machette et al., submitted manuscript, 2007]. *Knott et al.* [2002] showed that alluvial fan deposits in southern Death Valley with the characteristic Q2 morphology are younger than the late Pleistocene Lake Manly deposits dated at 180 to 120 ka by *Ku et al.* [1998]. In northern Death Valley, *Klinger* [2002] mapped deposits with the characteristic Q2 morphology that he subdivided into three units (Q2a, Q2b and Q2c) based on height above the active channel. At Red Wall and Big Dip Canyons, the Q2c unit is the only Q2 deposit preserved, and therefore our study is focused on the Q2c surface.

[13] Clasts on the Q2c fan surface range in size from cobble to small boulder and consist predominantly of carbonates and quartzites surrounded by tightly packed pebbles and small cobbles forming a mature desert pavement. The Q2c morphology is characterized by subdued to nonexistent bar and swale topography and a well-developed

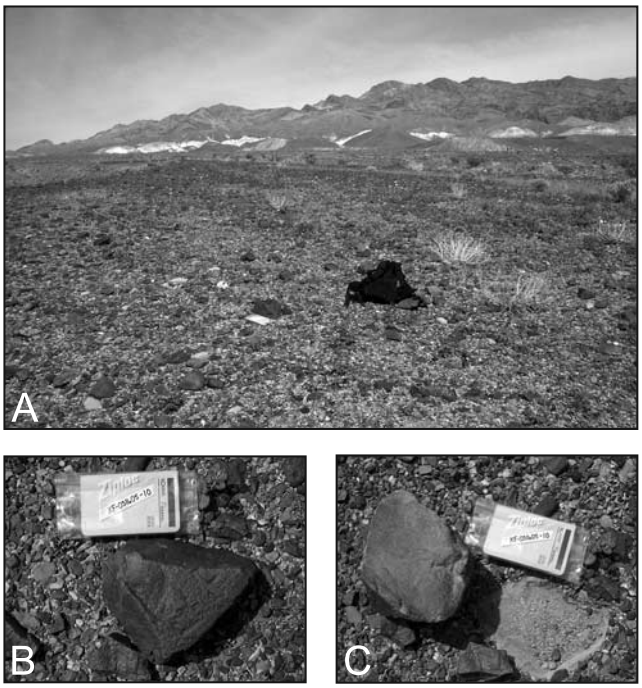

Figure 3. (a) View looking to the northeast across the Q2c surface of the Red Wall Canyon alluvial fan. Grapevine Mountains define the horizon. Notice the well-developed pavement and heavily varnished clasts on the smooth Q2c surface with subdued bar and swale topography. Daypack for scale. (b) Representative example of sample collected from the Q2c surface for ^{10}Be geochronology. Notebook for scale. (c) Underside of the sample in Figure 3b, showing the highly rubified nature of clasts on the Q2c surface and silty, vesicular A horizon commonly developed beneath clasts.

desert pavement. The tops of clasts are heavily varnished whereas the undersides are highly rubified (Figure 3). At Red Wall and Big Dip canyons the alluvial fans are composed of poorly sorted massive carbonate and quartzite breccias and conglomerates that are characteristic of debris flows [*Bull*, 1972].

[14] A mature soil, as much as 50-cm-thick, is developed below the Q2c surface (Figure 4). The soil is characterized by a 10- to 20-cm-thick Av horizon with clay film accumulation in its lower half; a middle Bt horizon with carbonate and salt development; and a lower Bk horizon with moderate carbonate accumulation (stage III) [*Birkeland*, 1999; *Klinger*, 2001]. On the basis of these characteristics, *Klinger* [2001] estimated that Q2c was deposited between 35 ka and 60 ka.

[15] Owing to its low relief, high degree of varnish, and well-developed soil, the Q2c surface stands out in marked contrast to its surrounding deposits, making it a perfect candidate for fault displacement reconstructions [*Frankel and Dolan*, 2007]. The Q2c surface has been incised and isolated by younger alluvial channels. Thus restoring slip by realigning channels incised through the Q2c surface provides a minimum slip rate over a late Pleistocene timescale.

[16] While we cannot address the potential for spatial variations in slip rates in this region from this site alone, the Red Wall Canyon alluvial fan provides the single best location for a long-term slip rate study on the NDVFZ. The Red Wall Canyon fan preserves multiple well-defined piercing points, excellent fault zone exposure along a single trace, and is characterized by the most stable geomorphic surface in the region, making it the most amenable site for cosmogenic nuclide geochronology (Figure 5). Furthermore, the offsets at Red Wall Canyon are at similar latitude to slip rate locations on the Owens Valley, Hunter Mountain, and Stateline faults (Figure 2), which allows us to calculate a robust long-term slip rate budget across the region.

4. Airborne Laser Swath Mapping and Fault Offset

4.1. Airborne Laser Swath Mapping Data Collection

[17] An important component of our study is the acquisition of airborne laser swath mapping (ALSM; also known as

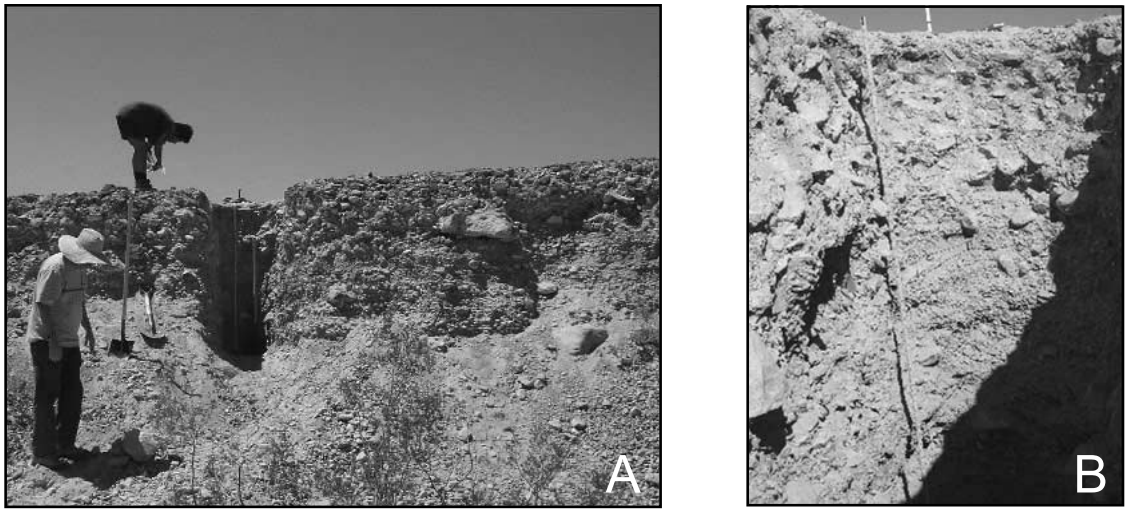

Figure 4. (a) Photograph looking north toward a channel wall exposure of the Big Dip Canyon alluvial fan, ~5 km north of Red Wall Canyon. The vertical channel in the photograph is the sample location of ^{36}Cl depth profile NRWF. (b) Photograph of a typical soil profile developed in Q2c surfaces in Death Valley. The tape measure provides a scale. Example shown is from the NRWF depth profile location.

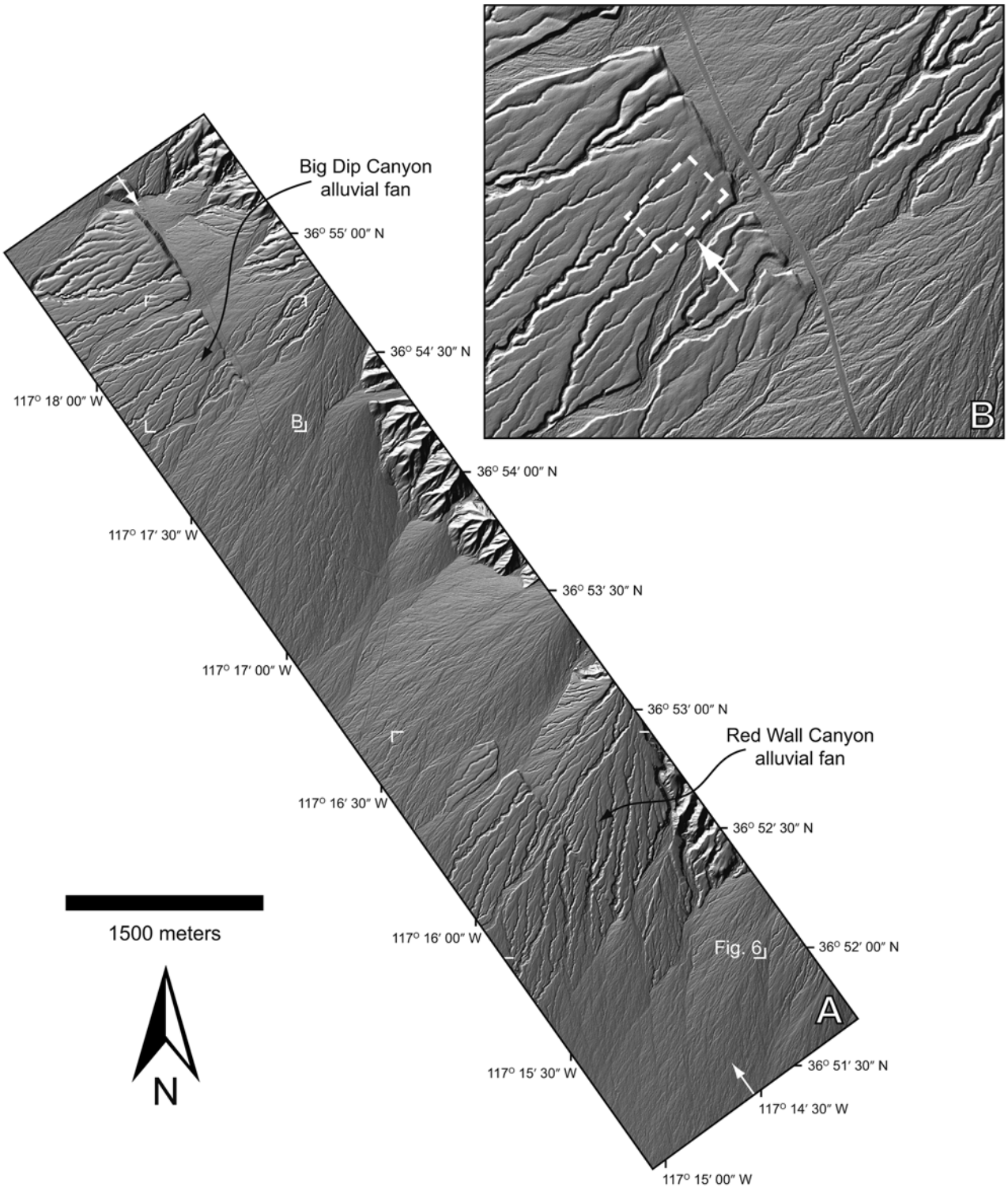

Figure 5. (a) Airborne laser swath mapping (ALSM) images of the study area. Location of strip map is shown by white box in Figure 2. White arrows delineate the surface trace of the northern Death Valley fault zone. The Red Wall Canyon alluvial fan is located in the southeast half of the image, and the detailed map in Figure 6 is outlined by the white box corners. (b) Detailed image of sample locations on the Big Dip Canyon alluvial fan. Arrow points to location of the depth profile collected from this site. White box indicates the region where the six surface samples were collected.

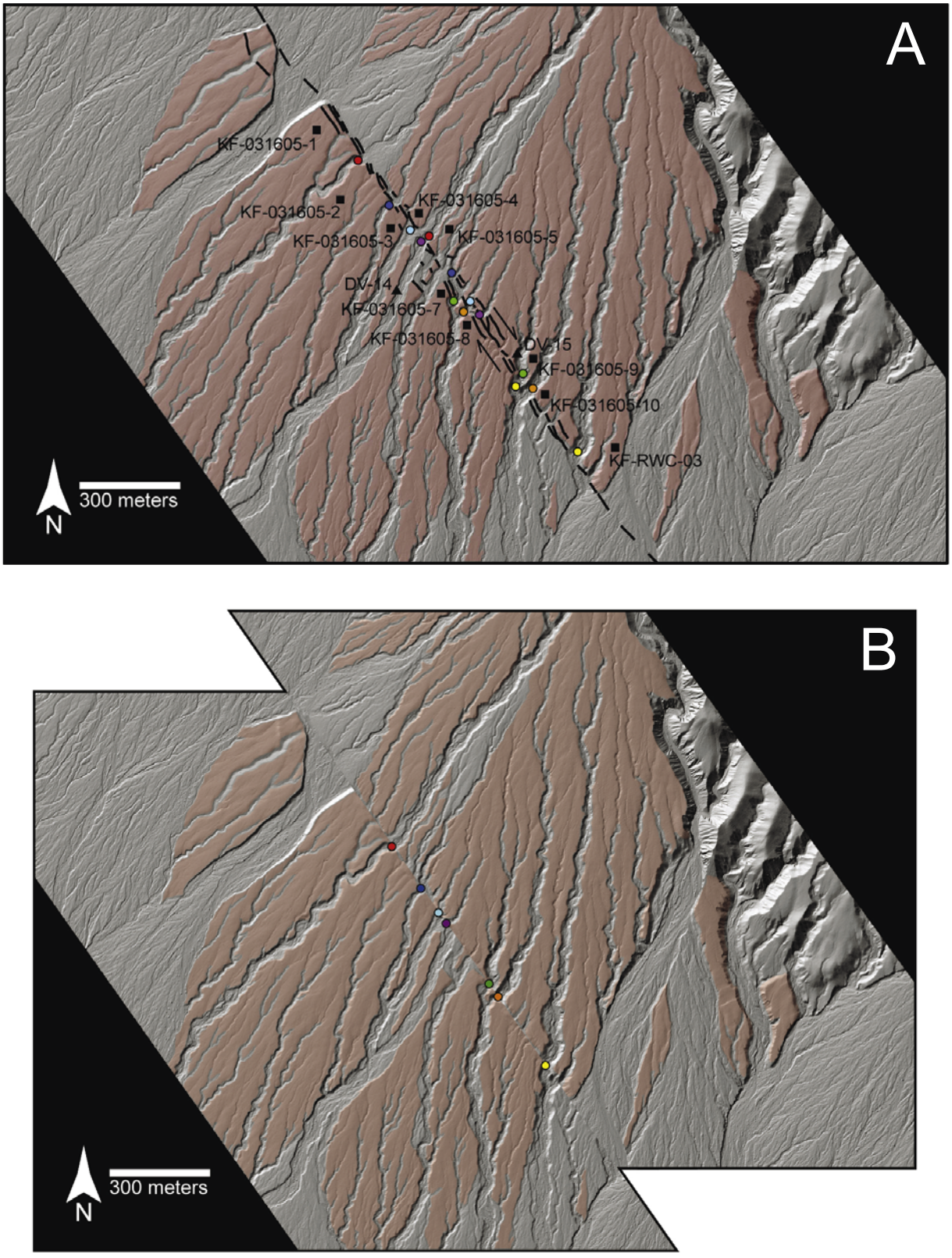

Figure 6. (a) Color-coded airborne laser swath mapping (ALSM) image of the Red Wall Canyon alluvial fan. The Q2c (oldest) surface is shown in red. Beryllium 10 surface sample locations are shown by black squares. Chlorine 36 depth profile locations are shown by black triangles. Colored circles indicate channels that correlate to each other when offset is restored. (b) ALSM image of Red Wall Canyon alluvial fan restored 297 ± 9 m to its original, prefaulting configuration. Colored circles mark the correlation of channels shown in Figure 6a. Q2c surface is shown in red. Geology is based on mapping by *Klinger* [2001]. See Table 1 for individual channel offset measurements.

Table 1. Channel Offset Measurements for Red Wall Canyon Alluvial Fan

Channel[a]	Thalweg Offset,[b] m	NW Riser Offset,[b] m	SE Riser Offset,[b] m
Red	307	303	304
Dark blue	291	291	285
Light blue	304	308	304
Purple	286	290	289
Green	301	304	294
Orange	306	301	303
Yellow	287	275	284

[a]Channel colors correspond to circles in Figure 6.
[b]Channel offsets and errors are taken as the mean and standard deviation of each set of measurements.

lidar) digital topographic data along the NDVFZ (Figure 5). The data were collected from an Optech Inc. Model ALTM 1233 laser mapping system. The laser was flown over the field area at an elevation of 600 m above ground level at an average speed of 60 m s^{-1} using a Cessna 337 twin engine aircraft. The aircraft was equipped with a dual-frequency geodetic quality GPS receiver and a real time display of the flight path and data coverage. The laser source produced 33,000 laser pulses per second and recorded the first and last returns of each pulse, as well as the relative intensity of each return. Processing of these data using SURFER (Golden Software) Version 8.04 with a kriging algorithm allowed the construction of a highly precise digital elevation model with 5 to 10 cm vertical accuracy and one-meter horizontal resolution [*Carter et al.*, 2001, 2003; *Sartori*, 2005].

4.2. Red Wall Canyon Alluvial Fan Offset

[18] The ALSM data collected from our field area clearly show seven dextrally offset alluvial channels on the Red Wall Canyon alluvial fan (Figures 5 and 6a). The high-resolution digital elevation data allow us to precisely reconstruct the offset alluvial fan to its prefaulting position (Figure 6). The ALSM data were processed in ArcInfo to produce hill-shaded relief maps and slope maps to aid in the identification, mapping, and reconstruction of offset landforms.

[19] Channel offsets were measured directly from the DEM in ArcInfo using the thalweg of each channel as a piercing point. Thalwegs were defined by constructing a channel network from the DEM where the deepest part of the channel is determined by routing the flow direction from each cell in the channel to its steepest downslope neighbor [e.g., *Tarboton et al.*, 1991]. This allows for the objective delineation of thalwegs, and thus piercing points, from which we were able to restore slip on the fault. The total amount of along-strike offset for the channel thalwegs ranges from 286 to 307 m (Table 1). The mean offset of the channels incised into the Q2c surface at the Red Wall Canyon alluvial fan is 297 ± 9 m. We use the mean and standard deviation of all measured offsets as the total post-Pleistocene fault displacement and error, respectively. This is a revision of the 250 to 330 m of displacement estimated by *Klinger* [2001] using low Sun angle 1:12,000-scale aerial photographs.

[20] As a test of the offset measurements determined from the thalwegs, offsets were also measured based on the northwest and southeast channel walls. This was accomplished by deriving a slope map from the high-resolution DEM so that channel walls were more readily defined and easier to match with one another. Although somewhat more subjective than the thalweg method described above, the results are nearly identical. Restoration of the northwest channel walls produced an offset of 296 ± 11 m, while the southeast margins are offset 294 ± 9 m (Table 1). Because of the more objective nature of the thalweg offsets, we use that as our preferred late Pleistocene displacement.

[21] No offset measurements were determined for the Big Dip Canyon alluvial fan. This fan does not have a correlative deposit preserved on the northeast side of the fault, and therefore slip cannot be restored to determine fault displacement at this location (Figure 5).

5. Terrestrial Cosmogenic Nuclide Geochronology

[22] The accumulation of terrestrial cosmogenic nuclides, produced by the interaction of cosmic rays with minerals at the Earth's surface, allows the age and history of geomorphic surfaces and deposits to be quantified [*Lal*, 1991; *Gosse and Phillips*, 2001]. Cosmogenic nuclides are particularly advantageous over techniques such as radiocarbon in regions that either lack datable organic matter, or where the anticipated age of such surfaces and deposits is greater than ~40 ka.

[23] For materials that contain no terrestrial cosmogenic nuclides at the time of formation (e.g., lava flows), the nuclide inventory is a function of only the time of exposure and erosion rate (please see the auxiliary material). In that case, the exposure age can generally be calculated based on a very limited number of samples. However, for samples from alluvial fans where inheritance is typically large, too many unknowns exist to uniquely solve the production equation. This problem can be overcome by collecting subsurface samples in a depth profile [*Anderson et al.*, 1996; *Repka et al.*, 1997; *Hancock et al.*, 1999]. Collecting samples at multiple depths allows the inherited component of the total cosmogenic-nuclide inventory to be separated from the in situ component [*Anderson et al.*, 1996; *Hancock et al.*, 1999; *Gosse and Phillips*, 2001].

5.1. Beryllium 10 Surface Samples

[24] Beryllium 10 is produced through spallation and muon-induced reactions with Si and O. Typically, quartz is used as the target mineral for ^{10}Be because of its stoichiometric simplicity, quantitative retention of ^{10}Be, and resistance to chemical weathering [*Gosse and Phillips*, 2001]. Sixteen surface samples from quartzite boulders and large cobbles were collected for the analysis of in situ cosmogenic ^{10}Be (Figures 3, 5, and 6). Ten samples were collected from stable surfaces close to the fault across the midsection of the Red Wall Canyon fan (Figure 6). Samples from Big Dip Canyon were collected in close proximity to each other from the most stable and least incised part of the fan surface near the location of the ^{36}Cl depth profile (Figure 5). The samples were resting on a Av soil horizon, were coated with a dark desert varnish on the top, showed rubification on the underside, and lacked carbonate collars or varnish alteration above the soil/clast interface. All of these features are characteristic of clasts that have resided at the

Table 2. Analytical Results of ^{10}Be Geochronology

Sample	Location, Latitude/Longitude	Altitude, m	Quartz,[a] g	Thickness, cm	Be Carrier,[b] g	^{10}Be/^{9}Be, 10^{-12}	Measured ^{10}Be,[c] 10^6 atoms (g SiO_2)$^{-1}$	^{10}Be Model Age,[d] years
KF-031605-1	36°52.20/117°15.60	401	30.04	5	0.7684	1.8440 ± 0.0292	1.379 ± 0.022	219,400 ± 3,500
KF-031605-2	36°52.58/117°15.75	393	30.04	5	0.7556	0.6673 ± 0.0155	0.491 ± 0.011	76,900 ± 1,800
KF-031605-3	36°52.53/117°15.63	391	30	5	0.7288	1.1220 ± 0.0221	0.797 ± 0.016	124,000 ± 2,400
KF-031605-4	36°52.57/117°15.59	398	30.03	5	0.877	0.4678 ± 0.0178	0.399 ± 0.015	62,500 ± 2,400
KF-031605-5	36°52.55/117°15.51	399	30	5	0.7602	0.6047 ± 0.0157	0.448 ± 0.012	70,000 ± 1,800
KF-031605-7	36°52.43/117°15.55	377	30.01	5	0.7626	0.5615 ± 0.0231	0.417 ± 0.017	65,200 ± 2,700
KF-031605-8	36°52.37/117°15.50	372	30.03	5	0.7605	0.6112 ± 0.0216	0.453 ± 0.016	70,800 ± 2,500
KF-031605-9	36°52.33/117°15.36	371	30.05	5	0.7621	0.7415 ± 0.0209	0.550 ± 0.015	86,400 ± 2,400
KF-031605-10	36°52.27/117°15.34	361	30.05	5	0.7586	0.6057 ± 0.0181	0.447 ± 0.013	69,900 ± 2,100
KF-RWC-03	36°52.20/117°15.20	355	30.04	5	0.7615	0.5990 ± 0.0179	0.444 ± 0.013	69,400 ± 2,100
Q2C-1	36°54.49/117°17.39	500	15.29	5	0.992	0.2837 ± 0.0921	0.538 ± 0.017	72,100 ± 2,300
Q2C-2	36°54.50/117°17.39	500	15.3855	5	0.9886	0.2224 ± 0.0817	0.418 ± 0.015	55,700 ± 2,000
Q2C-3	36°54.48/117°17.37	500	15.3095	5	0.984	0.3235 ± 0.0101	0.608 ± 0.019	81,900 ± 2,500
Q2C-4	36°54.48/117°17.35	500	15.3363	5	0.9965	0.2549 ± 0.0984	0.484 ± 0.019	64,800 ± 2,500
Q2C-5	36°54.46/117°17.37	500	15.2311	5	0.9933	0.2439 ± 0.0827	0.465 ± 0.016	62,300 ± 2,100
Q2C-6	36°54.48/117°17.33	500	14.9566	5	0.9899	0.1416 ± 0.0219	0.274 ± 0.042	36,500 ± 5,600

[a]A density of 2.7 g cm^{-3} was used for the quartzite surface samples.
[b]Be carrier concentration is 437 μg mL^{-1}.
[c]Propagated uncertainties include error in the blank, carrier, and counting statistics.
[d]Propagated error in the model ages include a 6% uncertainty in the production rate of ^{10}Be and 3% uncertainty in the ^{10}Be decay constant.

surface, relatively undisturbed, since deposition (Figure 3). The top 5 cm of each sample was cut away and only this portion of the clast was used for ^{10}Be extraction. The 5-cm-thick slabs were then crushed and sieved to separate the 250 to 500 μm grain size fraction. Pure quartz was then isolated by techniques outlined by *Kohl and Nishiizumi* [1992] and Be was extracted from the quartz by anion and cation exchange chromatography. Samples were then analyzed for ^{10}Be concentrations by accelerator mass spectrometry (AMS) at Lawrence Livermore National Laboratory. The 16 surface samples ranged in age from 37 ± 6 ka to 219 ± 4 ka; 12 of the 16 samples cluster between ~50 and 90 ka (Table 2). Sample ages were calculated using production rates of ^{10}Be based on the work by *Stone* [2000]. Carrier composition, counting statistics, and the blank are all potential sources of uncertainty in the measured ^{10}Be concentrations. A 3% error in the decay constant of ^{10}Be and 6% error in the production rates are propagated with the analytical uncertainties to produce errors on the ^{10}Be model age [*Stone*, 2000].

5.2. Chlorine 36 Depth Profile Samples

[25] Previous cosmogenic depth profile geochronologic studies show that locally sourced alluvial fan deposits in Death Valley typically contain a large inherited component in measured cosmogenic nuclide inventories [*Machette et al.*, 1999]. For this reason, three ^{36}Cl depth profiles were collected (1) to help determine the inherited signal in the Q2c surface and therefore better define the age of deformed landforms along the NDVFZ, and (2) as a direct comparison of two independent cosmogenic nuclide geochronologic techniques.

[26] Cosmogenic ^{36}Cl is principally produced in carbonate rocks and calcic soils by four reactions: high-energy spallation of K and Ca, epithermal neutron absorption by Cl, and thermal neutron absorption by Cl [*Gosse and Phillips*, 2001]. Chlorine 36 is also produced by muon-induced reactions, but the production rate in the top 2 m of alluvium is much less than for the reactions listed above [*Gosse and Phillips*, 2001]. The production rate at any depth below the surface by the first two reactions depends on the concentrations of the target elements and the high-energy cosmic ray flux at that depth. The high-energy cosmic ray flux decreases exponentially with the cumulative mass traversed by the cosmic rays. Thus production by these reactions can be calculated based on measurement of the bulk densities in the soil column at each sample depth and the concentrations of K and Ca in the sample material (please see auxiliary material Tables S1 and S2).

[27] Production by low-energy neutron absorption depends on the low-energy (thermal and epithermal) neutron fluxes and the Cl concentration (Table 3). However, low-energy neutrons are produced by gradual deceleration of the high-energy flux and they can diffuse significant distances while in the epithermal-thermal energy range. The characteristics of the low-energy flux thus depend on bulk properties of the medium [*Phillips et al.*, 2001].

[28] A total of 16 carbonate-rich samples from three depth profiles were collected from natural exposures in alluvial channel walls incised into Q2c deposits at the Red Wall Canyon and Big Dip Canyon alluvial fans (Figure 4). Two depth profiles were collected from the Red Wall Canyon alluvial fan and one depth profile was collected from the correlative alluvial fan surface at Big Dip Canyon (Figures 5 and 6). The soil profile at Big Dip Canyon is consistent with the soils described on the Q2c surface at Red Wall Canyon by *Klinger* [2002]. We excavated into the channel walls at least one meter to reduce possible lateral cosmic ray penetration (Figure 4). Approximately 150 clasts from the 5- to 15-mm-thick grain size fraction were collected from the alluvium in 10 to 15 cm thick sections distributed through the upper ~2 m of the alluvium, but below the Av horizon [*Phillips et al.*, 2003]. Sampling intervals increased with depth below the surface; samples were more closely spaced in the upper one meter of the profile, where a higher concentration of the cosmogenic ^{36}Cl resides. The clasts

Table 3. Analytical Results of ^{36}Cl Geochronology

Sample	Location, Latitude/Longitude	Elevation, m	Topographic Shielding Factor	Depth, m	^{36}Cl/Cl	Cl, ppm	Radiogenic ^{36}Cl, 10^{18} atoms g^{-1}	Cosmogenic ^{36}Cl, 10^{5} atoms g^{-1}
DV-14b	36°52.44/117°15.52	376	0.999	0.25	642 ± 12	77.79	1.32	8.5 ± 0.16
DV-14c	-	-	0.999	0.49	650 ± 12	93.80	1.59	10.0 ± 1.9
DV-14d	-	-	0.999	0.76	660 ± 13	79.77	1.35	8.9 ± 0.17
DV-14e	-	-	0.999	1.15	621 ± 21	95.67	1.62	9.8 ± 0.4
DV-14g	-	-	0.999	2.20	434 ± 15	67.14	1.14	5.0 ± 0.17
DV-15a	36°52.34/117°15.34	366	0.999	0.20	682 ± 20	104.00	1.77	12.0 ± 3.5
DV-15b	-	-	0.999	0.55	587 ± 22	86.46	1.47	8.4 ± 0.31
DV-15c	-	-	0.999	0.86	613 ± 23	57.95	0.98	5.9 ± 0.22
DV-15d	-	-	0.999	1.25	404 ± 13	78.96	1.34	5.3 ± 0.17
DV-15e	-	-	0.999	1.98	412 ± 12	102.24	1.74	7.0 ± 0.21
NRWF-0	36°54.65/117°17.67	488	0.999	0.05	1740 ± 70	25.52	0.43	7.5 ± 0.30
NRWF-15	-	-	0.999	0.15	1190 ± 29	49.19	0.84	9.9 ± 0.24
NRWF-35	-	-	0.999	0.40	1110 ± 83	44.94	0.76	8.4 ± 0.63
NRWF-70	-	-	0.999	0.75	896 ± 34	55.43	0.94	8.3 ± 0.32
NRWF-120	-	-	0.999	1.25	317 ± 150	31.47	0.53	1.6 ± 0.80
NRWF-180	-	-	0.999	1.85	883 ± 40	30.98	0.53	4.6 ± 0.21

were ground to fine sand size and carefully mixed to ensure a homogeneous sample.

[29] Aliquots of the sample were sent to the New Mexico Bureau of Mines and Mineral Resources X-ray fluorescence laboratory for analysis of major elements and U and Th, and to the XRAL Laboratory in Ontario, Canada, for gamma emission spectrometry analysis of B and Gd (see auxiliary material Table S1). Masses of the remaining sample material, ranging from 80 to 125 g, were dissolved to extract Cl using standard procedures [e.g., *Zreda*, 1994]. Samples were then sent to PRIME Lab at Purdue University for accelerator mass spectrometry analysis of the ^{36}Cl/Cl ratio and the ^{35}Cl/Cl ratio [*Elmore et al.*, 1979]. The spreadsheet program CHLOE (CHLOrine-36 Exposure age) was used to calculate the ^{36}Cl/Cl ratio and Cl concentration of the samples based on the ^{36}Cl/Cl and ^{35}Cl/Cl analyses, sample mass, and mass of added ^{35}Cl carrier (Table 3; please see description of CHLOE in auxiliary materials) [*Phillips and Plummer*, 1996].

[30] The soil age was determined by obtaining a best fit between a calculated ^{36}Cl inventory (as a function of depth) and the measured ^{36}Cl profile. The best fit match was identified by minimization of the sum of the χ^2 values, computed from the differences between the calculated and measured values at each depth, for all of the samples in the profile. Uncertainties in the ages were also calculated from the χ^2 variation. The theoretical ^{36}Cl inventories with depth were calculated using CHLOE (see auxiliary material) [*Phillips and Plummer*, 1996]. Production parameters given by *Phillips et al.* [2001] and *Stone et al.* [1998] are used in the model. Use of alternative production parameters by *Stone et al.* [1996a, 1996b] would give ages that are younger by 18%. Using inferred soil histories based on soil descriptions [*Klinger*, 2002; Machette et al., submitted manuscript, 2007] and the observed thickness of Av horizons, we estimated the amount of surface erosion or aggradation at each sampling site and used the cosmogenic ^{36}Cl concentrations in each depth profile to calculate maximum, minimum, and preferred surface erosion rates in mm ka^{-1}. The preferred erosion/aggradation rates range from 0 mm ka^{-1} (stable) to −0.7 mm ka^{-1} (7 cm of aggradation in 100 ka; Table 4).

[31] In Table 4 we report the best estimate depth profile ages with uncertainty bounds, best estimate erosion rate associated with that age, the reduced sum of χ^2 ($\chi\nu^2$), the range of aggradation/erosion rates employed in the analysis, the inheritance age (note that this reflects inheritance at the time of sampling, not deposition), and the calculated erosion rate in the source area. The two depth profiles from the Red Wall Canyon fan, DV-14 and DV-15, yielded ages of 65 +16/−10 ka and 55 +13/−16 ka, respectively. A single depth profile from the Big Dip Canyon fan produced an age of 75 +18/−16 ka. Two of the three profiles (DV-14 and DV-15) yield $\chi\nu^2$ values significantly less than one. These fits indicate that the CHLOE modeling approach is performing well in describing the cosmogenic nuclide accumulation processes and support the likelihood of a conservative bias in the uncertainty analysis. The third

Table 4. The ^{36}Cl Best Estimate Depositional Age, Depth Profile Erosion Rate, Reduced Sum of χ^2, Assumed Erosion/Aggradation Rate Bounds, Equivalent Inheritance Age, and Source Area Catchment-wide Erosion Rate

Depth Profile	Deposition Age, ka	Profile Erosion Rate, g cm^{-2} ka^{-1}	$\chi\upsilon^2$	Erosion/Aggradation Limits, g cm^{-2} ka^{-1} Lower Limit	Upper Limit	Inheritance Age, ka	Source Area Erosion Rate,[a] g cm^{-2} ka^{-1}	Source Area Erosion Rate,[b] mm ka^{-1}
DV-14	65 + 16/−10	−0.7	0.745	−0.7	0	59 ± 8	13 ± 2	46 ± 9
DV-15	55 + 13/−16	0	0.12	−0.7	0	63 ± 8	23 ± 3	83 ± 10
NRWF	75 + 18/−16	−0.35	3.97	−0.7	0	55 ± 20		

[a]Source area erosion not calculated for the alluvial fan 5 km north of Red Wall Canyon because the source area is not known.
[b]Calculated assuming a bedrock density of 2.65 g cm^{-1}.

profile (NRWF) has a $\chi\nu^2$ of 3.97, largely due to the anomalous sample at 1.25 m depth.

[32] In addition, we determined source area erosion rates (i.e., the erosion rate in the mountain range from which the debris flows were derived) using the estimated inheritance of each profile. This assumes that the sediment in the profiles was derived directly from bedrock erosion in the source area catchment, without long-term storage in the drainage that could result in additional cosmogenic nuclide production during transit. The erosion rate was calculated using a weighted mean elevation/latitude scaling factor (S_{el}) derived by obtaining the hypsometry of the drainage basin upstream of the apex of the Red Wall Canyon alluvial fan from a 30-m-resolution DEM in ArcInfo and weighting the S_{el} in each elevation class by its relative area. CHLOE was then used to calculate the steady state erosion rate that would produce the observed inherited ^{36}Cl inventory for each profile. The calculated late Quaternary source area catchment-wide erosion rates range from 46 ± 9 mm ka^{-1} to 83 ± 10 mm ka^{-1} and are somewhat slower than Holocene erosion rates estimated along the Black Mountains normal fault in central Death Valley (Table 4) [*Frankel et al.*, 2004; *Jayko*, 2005].

6. Discussion

6.1. Terrestrial Cosmogenic Nuclide Geochronology

6.1.1. Beryllium 10

[33] Surface exposure dates for the Q2c surface obtained from ^{10}Be concentrations in quartzite clasts on two alluvial fans along the NDVFZ yield ages with a range of ~183 ka, from ~37 to 219 ka (Table 2). This relatively large variance is not surprising given that *Machette et al.* [1999, also submitted manuscript, 2007] report large inherited components of cosmogenic isotopes in other Death Valley alluvial fans. Nevertheless, this apparently disparate data set can be reconciled by plotting a probability density function of the distribution of ages (Figure 7). On the basis of visual inspection alone, one can pick out four peaks in the distribution shown by Figure 7c. The pronounced peak centered on ~70 ka is the most obvious and comprises 13 samples, 80% of those dated. Of the three outlying peaks, two are significantly older and one is somewhat younger.

[34] To the right of the main peak, two outliers exist, representing samples KF-031605-1 and KF-031605-3. It is clear that these outlying samples have anomalously high concentrations of ^{10}Be. The elevated ^{10}Be concentrations likely result from an inherited cosmogenic signal possibly due to protracted exposure on hillslopes prior to being eroded or during transport. We feel these samples should therefore not be considered to reflect the age of this fan deposit. Similarly, to the left of the large peak an anomalously young sample is observed in Figure 7. There are several likely scenarios to explain the young age of this sample including the possibilities that the boulder may have been dislodged, broken, or rotated in such a way that different clast surface geometries were exposed to cosmic rays with the varnish, rubification and Av horizon subsequently reestablished. Alternatively, the boulder may have been exhumed from beneath the surface by human or animal activity after the landform stabilized. Regardless, we feel this sample is not representative of the surface age, and therefore dismiss it.

[35] The highest peak in the probability density function in Figure 7c is used to represent the ^{10}Be age of the offset Q2c surface. The large cluster of ages centered on this peak suggests little or no inheritance in these samples. On the basis of ^{10}Be concentrations, the width of the distributions on either side of the highest probability not including the obvious outliers (i.e., ~50 ka and 92 ka), is considered to set a conservative bound on the uncertainty associated with the age of the surface (Figure 7). This corresponds to a ^{10}Be model age of 70 +22/−20 ka. This age is consistent with the 35 to 60 ka range estimated by *Klinger* [2001] on the basis of soil development and alluvial fan morphology and the 180 to 120 ka ages of the stratigraphically older Lake Manly deposits [*Ku et al.*, 1998].

6.1.2. Chlorine 36

[36] The ^{36}Cl age calculated from depth profiles beneath the offset Q2c surface are commensurate with the age determined by the cosmogenic ^{10}Be geochronology. The two depth profiles from the Red Wall Canyon alluvial fan (DV-14 and DV-15) yield ages of 65 +16/−10 ka and 55 +13/−16 ka (Figures 8a and 8b). Chlorine 36 inheritance of 59 ± 8 ka and 63 ± 8 ka were removed from each profile, respectively in calculating the surface ages. The depth profile collected from Big Dip Canyon produced an age of 75 +18/−16 ka (Figure 8c). Approximately 55 ka of ^{36}Cl inheritance was removed from this depth profile.

[37] The ^{36}Cl model age for Q2c was determined by calculating a weighted mean of the three depth profiles. The uncertainty of the weighted mean age was taken to be the square root of the geometric mean of the squared standard deviation of uncertainties in each sample [*Bevington and Robinson*, 2003]. This allows us to account for a reduction in the uncertainty due to combining three sets of data. The resulting weighted mean ^{36}Cl model age of the three depth profiles on Q2c surface is 63 ± 8 ka. A weighted mean calculated using only the two Red Wall Canyon depth profiles (DV-14 and DV-15) produces a younger, but not significantly different, age of 60 ± 10 ka.

6.2. Comparison of ^{10}Be and ^{36}Cl Geochronology

[38] After the removal of inheritance from the ^{36}Cl depth profiles, the 63 ± 8 ka ^{36}Cl and 70 + 22/−20 ka ^{10}Be ages are in relatively good agreement. However, it is difficult to reconcile the large inherited component observed in the ^{36}Cl depth profile ages compared with the ^{10}Be surface ages, which have relatively minor inheritance. Although the processes governing the discrepancy in cosmogenic nuclide inventories between the ^{10}Be and ^{36}Cl samples are not well understood, we propose that a likely explanation for this disparity may reside in the greater than order of magnitude difference in sampled clast size [e.g., *Brown et al.*, 1998; *Matmon et al.*, 2003; *Belmont et al.*, 2006].

[39] For example, it is easy to imagine a scenario for the large cobbles and boulders where the time between hillslope exposure (if, in fact, the samples were exposed on the hillslope at all), erosion, transport, and deposition is short. In arid regions, like Death Valley, weathering-resistant lithologies produce steep slopes and large clasts in the source area [*Harvey*, 1997]. Both clasts that are exposed at the surface and those that have remained completely

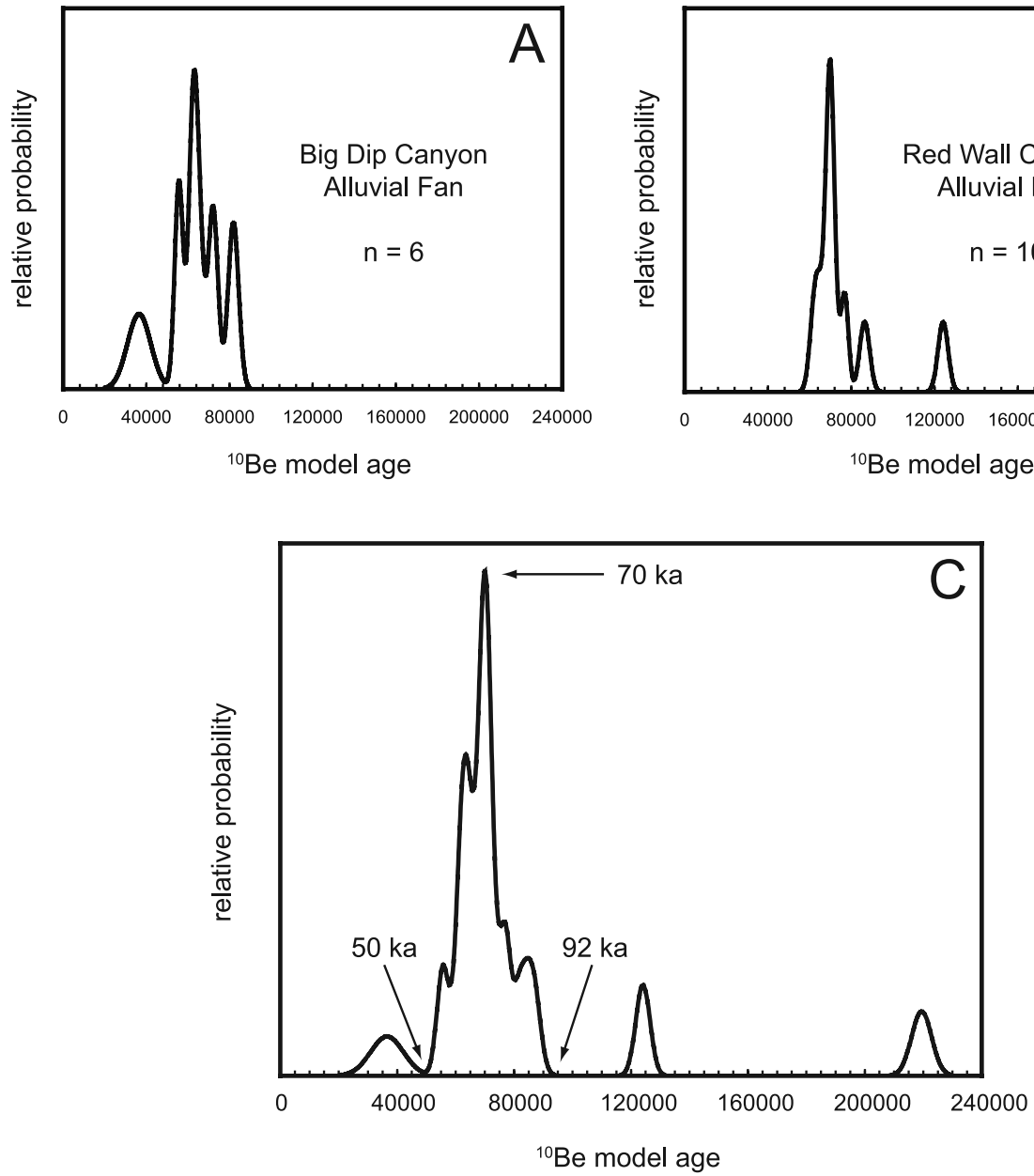

Figure 7. Probability density functions of the ^{10}Be ages from surface clasts, calculated using Isoplot [*Ludwig*, 2003]. (a) Probability density function of the six ages determined for the correlative Q2c surface on the Big Dip Canyon alluvial fan. (b) Probability density function of the 10 ages for the Q2c surface on the Red Wall Canyon alluvial fan. (c) Combined probability density function of all samples in Figures 7a and 7b. The age of the Q2c surface based on the combined dates between 50 and 92 ka is 70 + 22/−20 ka.

shielded would be transported from source to depocenter in rapid, single events. In this case, clasts would be removed from hillslopes by advective (landsliding and nonlinear creep) processes and transported by debris flows where the large clasts would remain intact and do not have time to undergo chemical or mechanical weathering before, or during, deposition.

[40] Conversely, clasts collected from the subsurface in the depth profiles are of considerably smaller grain size. These samples were likely exposed for long periods of time on hillslopes, as the relatively slow catchment-wide erosion rates suggest, where they would be exposed to increased chemical and mechanical weathering, resulting in grain by grain dissociation and slow, diffusive transport from hillslope to channel. Once in the channel network, these grains would be subject to the characteristic episodic precipitation of arid regions, which tends to generate steep rising limb hydrographs with short lag times that result in high suspended load transport and reworking of sands and gravels from alluvial fan channels [*Bull*, 1991; *Reid and Frostick*, 1997]. The hypothesis that the fine-grained component of alluvial fan deposits contains large amounts of inherited cosmogenic nuclides is supported by ^{36}Cl measurements on modern alluvial channel sands from four canyons on the

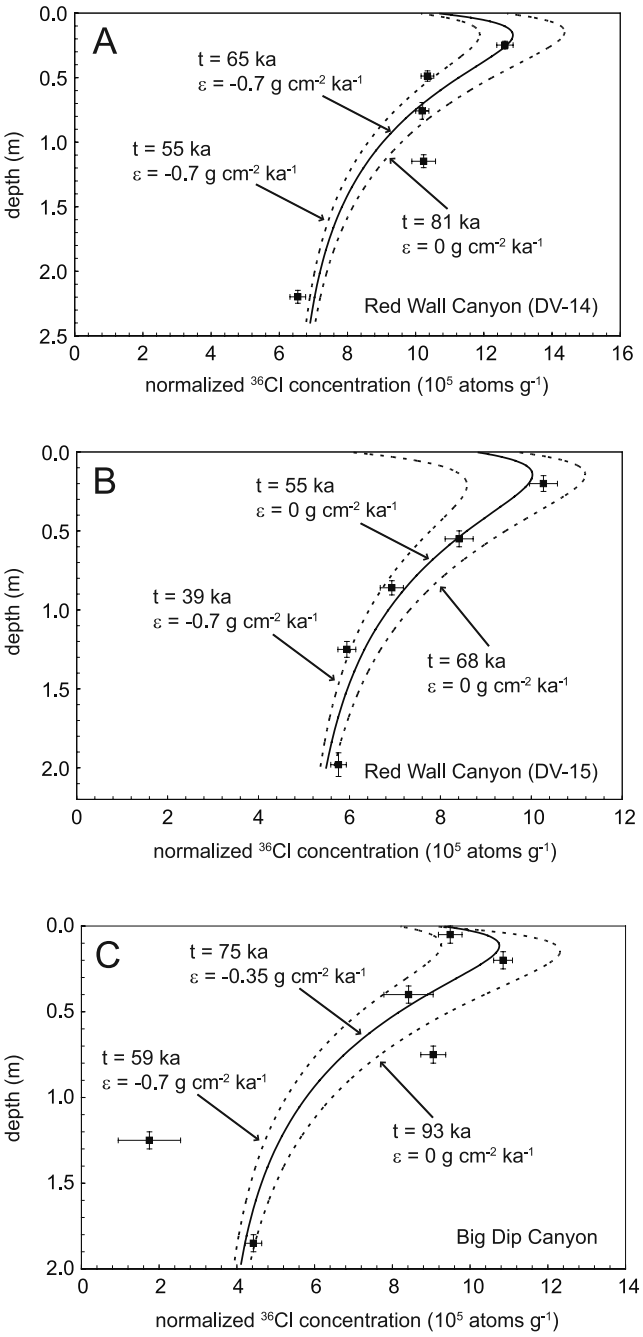

Figure 8. Normalized ^{36}Cl concentrations as a function of depth. (a) Profile DV-14 from Red Wall Canyon alluvial fan. (b) Profile DV-15 from Red Wall Canyon alluvial fan. (c) Profile NRWF from Big Dip Canyon alluvial fan. The solid lines indicate the calculated best fit profile, and the dashed lines indicate the calculated profiles for the 1σ upper and lower bounding age estimates; t is the depositional age, and ε is the erosion/aggradation rate used to calculate the profiles. Positive values of ε represent erosion, and negative values of ε represent aggradation. Note that although normalized concentration profiles are shown for purposes of illustration, the fitting was performed using actual measured concentrations and chemical compositions at each depth. See auxiliary materials for a detailed explanation of how ages were calculated from the depth profiles. Locations of the depth profiles are shown in Figures 5 and 6.

west side of Death Valley by Machette et al. (submitted manuscript, 2007). These modern sand fraction samples contain ^{36}Cl inheritance equivalent to 38 to 83 ka worth of exposure.

[41] Although *Clapp et al.* [2000, 2002] have previously suggested that no relationship exists between grain size and cosmogenic nuclide concentrations in arid environments, they did not take into account the wide range of grain sizes presented here. The significant differences in cosmogenic nuclide inventories between the two grain sizes analyzed in this study clearly reflect the underlying form and process of the arid region alluvial fan erosion-deposition system. Additional work on this subject is obviously warranted and will, in all likelihood, improve our understanding of denudation processes and interpretation of cosmogenic nuclide geochronologic data [e.g., *Belmont et al.*, 2006].

6.3. Fault Slip Rates

[42] The ^{10}Be and ^{36}Cl ages for the Q2c surface are, in effect, maximum ages for calculating slip rates because the channels used as piercing points must have developed after abandonment of the surface. Therefore the ages provide a minimum slip rate estimate. The ^{10}Be ages are used as the maximum limiting age of the offset Q2c surface because these data are likely to have only a small amount of inheritance. The measured 297 ± 9 m offset of this surface over a 70 +22/−20 ka time period yields a slip rate of 4.2 +1.9/−1.1 mm yr^{-1}. These data therefore provide a minimum slip rate for the NDVFZ. The age of the Q2c surface based on the weighted mean age of three ^{36}Cl depth profiles is taken to be a minimum bound on the age of the offset Q2c surface because we have been able to remove the inherited component from these samples. Using a minimum age of 63 ± 8 ka, the slip rate based on the cosmogenic ^{36}Cl geochronology is 4.7 +0.9/−0.6 mm yr^{-1}, which is in agreement with the slip rate derived from the ^{10}Be geochronology. The average of the two rates is 4.5 mm yr^{-1}. Using the bounding error limits for both rate calculations yields a geologic slip rate of 3.1 to 6.1 mm yr^{-1} (4.5 +1.6/−1.4 mm yr^{-1}) for the NDVFZ at the Red Wall Canyon site.

[43] Because our slip rate is based on a single site along the NDVFZ we cannot address the potential for along-strike variations in slip rates in this region. However, we note that a number of previous studies indicate slip distributions are commonly asymmetric, with the largest displacements often occurring near one end of the fault [e.g., *Wesnousky*, 1988; *Ellis and Dunlap*, 1988; *Peacock and Sanderson*, 1991; *Cartwright and Mansfield*, 1998; *Maerten et al.*, 1999; *Manighetti et al.*, 2001, 2005], and thus our study site is not necessarily located at the point of greatest cumulative displacement on the NDVFZ. Indeed, the long-term rate may increase to the north as slip is transferred from the Tin Mountain and Deep Springs faults onto the northern Death Valley and Fish Lake Valley fault zones (Figure 2) [e.g., *Dixon et al.*, 1995; *Reheis and Dixon*, 1996].

[44] Nevertheless, the slip rates derived from cosmogenic nuclide geochronology at Red Wall Canyon are consistent with the 3 to 9 mm yr^{-1} slip rate estimate of *Klinger* [2001] and with recent geodetic estimates of elastic strain accumulation on the Death Valley fault system [*Bennett et al.*, 1997; *Gan et al.*, 2000; *Dixon et al.*, 2003; *Wernicke et al.*, 2004].

Table 5. Fault Slip Rates in the Northern Eastern California Shear Zone[a]

Fault	Geologic Rate, mm yr^{-1}	Time Period	Method Used to Estimate Geologic Rate	Geodetic Rate, mm yr^{-1}
Northern Death Valley	3.1–6.1(1)	late Pleistocene	cosmogenic nuclides (1)	3–9.5 (2–7)
Saline Valley–Hunter Mountain	3.3–4.0 (8)	late Pleistocene	soil development (8)	1.7–4.9 (2–7)
Owens Valley	0.7–3.8 (9–11)	late Pleistocene to Holocene	optically stimulated luminescence (11)	1.8–8 (2–7, 12, 13)
Stateline	1–2 (14, 15)	post-mid-Miocene	correlation of dated volcanic breccia (15)	0.9–1.4 (16)
Northern ECSZ (range)	8.1–15.9 (1)	late Pleistocene to present		7.4–23.8 (2–7, 12, 13, 16)
Northern ECSZ (best estimate)	8.5–10 (1)	late Pleistocene to present		9.3 ± 0.2 (17)

[a]References (indicated in parentheses) are 1 [this study]; 2, *Dixon et al.* [1995]; 3, *Bennett et al.* [1997]; 4, *Gan et al.* [2000]; 5, *Miller et al.* [2001]; 6, *McClusky et al.* [2001]; 7, *Dixon et al.* [2003]; 8, *Oswald and Wesnousky* [2002]; 9, *Lubetkin and Clark* [1988]; 10, *Beanland and Clark* [1994]; 11, *Lee et al.* [2001b]; 12, *Savage et al.* [1990]; 13, *Savage and Lisowski* [1995]; 14, *Schweickert and Lahren* [1997]; 15, *Guest et al.* [2005]; 16, *Wernicke et al.* [2004]; 17, *Bennett et al.* [2003].

We also note that the midrange of our estimate of 4.5 mm yr^{-1} is <50% higher than the geodetic rate of 2.8 mm yr^{-1} suggested by *McClusky et al.* [2001] and *Wernicke et al.* [2004]. Our data, when combined with published rates on the other three major right-lateral faults (Owens Valley, Hunter Mountain, and Stateline) at the same latitude in this part of the ECSZ provides the first synoptic view of the cumulative slip rate across the ECSZ, north of the Garlock fault (Table 5 and Figure 2).

[45] *Oswald and Wesnousky* [2002] report a right-lateral slip rate along the HMFZ of 3.3 to 4 mm yr^{-1} on the basis of 50 to 60 m of offset across a ~15 ka surface. On the basis of low-temperature thermochronologic data, *Lee and Stockli* [2006] suggest a similar rate for the HMFZ since the Pliocene. We use 3.3 mm yr^{-1} for the HMFZ in this study because it provides us with a minimum slip rate for this fault. The OVFZ, site of the most recent major earthquake in the northern half of the eastern California shear zone (M_w ~7.6 in 1872), has a range of Holocene slip rates from 0.7 to 3.8 mm yr^{-1} [*Lubetkin and Clark*, 1988; *Beanland and Clark*, 1994; *Lee et al.*, 2001b]. For this study, we use the 1.2 mm yr^{-1} slip rate for the OVFZ determined by *Lee et al.* [2001b] based on offset early Holocene channels dated by optically stimulated luminescence geochronology. This rate is close to the mean of the other rates reported for the OVFZ and is the only rate reported for the OVFZ where a geochronologically determined age of the offset landform is known. We take the 1 mm yr^{-1} to be the best estimate for the geologic slip rate on the SLFZ [*Schweickert and Lahren*, 1997; *Wernicke et al.*, 2004; *Guest et al.*, 2005]. While *Guest et al.* [2005] report a post-mid-Miocene slip rate of ~2 mm yr^{-1} for the SLFZ, the subtle geomorphic expression of the fault in alluvial deposits suggests the late Pleistocene to Holocene rate is somewhat lower.

[46] Summing the slip rates from the Owens Valley, Hunter Mountain, and Stateline fault zones with the slip rate determined for the NDVFZ in this study yields a total long-term geologic slip rate of 8.1 to 15.9 mm yr^{-1} across the northern ECSZ (Table 5 and Figure 2). Using 1.2, 3.3, 4.5, and 1 mm yr^{-1} as the preferred slip rates for the OVFZ, HMFZ, NDVFZ, and SLFZ, respectively, the total geologic slip rate across the northern ECSZ at latitude ~37°N is 8.5 to 10 mm yr^{-1} (Table 5). Recent geodetic measurements suggest 9.3 ± 0.2 mm yr^{-1} of dextral shear across this region [*Bennett et al.*, 2003], which is indistinguishable from our best estimate of the geologic slip rate (Table 5). However, if we take our preferred geologic slip rate estimates for the OVFZ, HMFZ, and NDVFZ a strong skewing of the strain rate toward the east is predicted. This pattern is not observed in the geodetic data and may be the result of a secular slowing or transfer of strain from east to west across the region [e.g., *Wernicke et al.*, 2005]. Alternatively, the effects of postseismic processes, such as those resulting from the 1872 Owens Valley earthquake, could play a role in the observed pattern of elastic strain accumulation [*Pollitz and Sacks*, 1992; *Dixon et al.*, 2003]

[47] The cosmogenic nuclide geochronology and ALSM data presented here are fundamental for estimating a long-term geologic fault slip rate on the NDVFZ, an important piece to the slip rate "puzzle" in the northern ECSZ. A more quantitative estimate on the dextral motion of the HMFZ, in addition to the down-to-the-northwest extensional faults linking the strike-slip systems, would produce even tighter bounds on the long-term distribution of strain in this region. Even so, strain release in the northern ECSZ averaged over at least 50,000 to 100,000 years is consistent with the overall rate of strain accumulation as measured by short-term (5 to 10 years) geodetic data. However, the fact that the geologic estimates partition most of the strain (~85%) on to the HMFZ and NDVFZ does not agree with the relatively constant strain rate of 60 nstrain yr^{-1} measured across the entire ECSZ [*Bennett et al.*, 2003], indicating that seismic cycle or other effects are at work. Although outside the scope of this study, questions still remain as to the spatial and temporal constancy of strain accumulation and release along major strike-slip fault systems, such as the NDVFZ, and future work in the region should focus on this.

7. Implications for Eastern California Shear Zone Kinematics

[48] Strain accumulation and release appear to be relatively constant over a wide range of timescales on at least parts of the few major faults where sufficiently detailed geologic rate data are available, such as the central San Andreas fault [*Sieh and Jahns*, 1984; *Argus and Gordon*, 2001]. In contrast, rates of strain release during the past ~1500 years on other parts of the San Andreas system vary by a factor of 4 due to the accumulation of strain over multiple seismic cycles [*Weldon et al.*, 2004]. Similarly, recent comparisons of geodetic and geologic rate data

across the Mojave section of the ECSZ appear to indicate a pronounced strain transient. Specifically, the geodetic rates measured in the region (12 ± 2 mm yr^{-1}) are almost twice as fast as the longer-term geologic rates (on the order of ~5 to 7 mm yr^{-1}) [*Dixon et al.*, 2000; *Rockwell et al.*, 2000; *McClusky et al.*, 2001; *Peltzer et al.*, 2001; *Oskin and Iriondo*, 2004; *Oskin et al.*, 2006, 2007].

[49] North of the Garlock fault, along the eastern margin of the ECSZ, continuous geodetic data from the Yucca Mountain area, Nevada, ~50 km NE of the NDVFZ, suggests that ~1 mm yr^{-1} of right-lateral shear across the area is not accommodated by any recognizable Quaternary structure [*Wernicke et al.*, 2004]. In the north central Basin and Range, some geodetic velocities across normal faults with late Holocene earthquakes indicate horizontal shortening, not extension [*Wernicke et al.*, 2000; *Friedrich et al.*, 2004]. These studies serve to highlight the phenomenon of transient strain accumulation.

[50] The preferred sum of the geologic slip rates on the Owens Valley, Hunter Mountain, Stateline and northern Death Valley fault zones at latitude ~37° N is 8.5 to 10 mm yr^{-1} (Table 4). Geodetic data indicate a similar amount of dextral shear across this region of 9.3 ± 0.2 mm yr^{-1} over a ~5 year period (Table 5) [*Bennett et al.*, 2003]. We note that our results indicate faster, long-term rates on the eastern faults in the study area. Previous geodetic studies report conflicting results when slip rates are modeled for individual faults in the northern ECSZ [*Gan et al.*, 2000; *Dixon et al.*, 2003]. *Gan et al.* [2000] suggest much faster rates on the westernmost fault in the system, the Owens Valley fault zone, which appears to have a much slower long-term rate [*Lee et al.*, 2001b]. Alternatively, *Dixon et al.* [2003] suggest the northern Death Valley fault zone accommodates the majority of slip in the region using a rate that is also much faster than the long-term geologic rate. The basic geodetic rate of 9.3 mm yr^{-1} across the entire ECSZ by *Bennett et al.* [2003] is robust; however, the details of individual faults are highly dependent on the model used to evaluate the geodetic data. Regardless, our results suggest that the transient strain accumulation proposed for the Mojave section of the ECSZ does not extend north of the Garlock fault.

[51] In the northern half of the eastern California shear zone, north of the Garlock fault and away from the zone of structural complexity in the Pacific–North America plate boundary, the far-field effect of the Big Bend of the San Andreas fault on strain accumulation and release is dampened. As a result, strain is more simply accommodated by translation of the rigid Sierra Nevada block to the north with respect to the western Basin and Range province and stable North America [*Argus and Gordon*, 2001; *Bennett et al.*, 2003]. Thus the dextral component of plate boundary deformation in this region is partitioned among the Owens Valley, Hunter Mountain, northern Death Valley, and Stateline fault zones, which together accommodate ~20% of total Pacific–North America plate motion.

8. Conclusions

[52] Comparison of longer-term geologic rate data with short-term geodetic data illustrates that the average rate of strain storage and release over the past ~70 ka is, within error, the same as the 5-year rate of elastic strain accumulation in the northern half of the ECSZ. The agreement between the short- and long-term rates suggests that the transient strain accumulation observed in the Mojave Desert is not present north of the Garlock fault. Although our interpretation depends on the choice of individual geologic fault slip rates, given the limited data currently available this study provides the first synthesis of slip rates in the northern ECSZ. Clearly more long-term slip rate studies are needed to test our suppositions.

[53] Fault slip rates determined from ^{10}Be and ^{36}Cl cosmogenic geochronology on offset alluvial fans on the NDVFZ zone agree between the two independent cosmogenic geochronometers, yielding independent rates of 4.2 +1.9/−1.1 to 4.7 +0.9/−0.6 mm yr^{-1}, respectively. A summation of slip rates on the Owens Valley, Hunter Mountain, northern Death Valley, and Stateline fault zones at latitude ~37° N implies that the long-term geologic slip rates across this region are similar to short-term geodetic rates over the northern ECSZ, both of which are ~9 mm yr^{-1}. However, the concentration of slip in the eastern portion of the shear zone on geological timescales is not consistent with the relatively constant strain rates measured from the eastern Sierra Nevada to central Nevada. These data suggest that the current strain transient observed in the Mojave section of the ECSZ [*Oskin and Iriondo*, 2004] may be a localized feature, likely tied to the zone of structural complexity associated with the Big Bend of the San Andreas fault [e.g., *Bartley et al.*, 1990; *Nur et al.*, 1993; *Du and Aydin*, 1996; *Li and Liu*, 2006; *Dolan et al.*, 2007], and may not be characteristic of the Pacific–North America plate boundary as a whole.

[54] **Acknowledgments.** We thank Patrick Belmont, David Bowman, Stephanie Briggs, Charles Sammis, and Jeremy Zechar for thought-provoking discussions. Patrick Belmont is also thanked for his assistance with field work. Permission to collect samples and access field sites within Death Valley National Park was granted by the Death Valley National Park Service Natural Resources Office. ALSM data were acquired by the National Center for Airborne Laser Swath Mapping (NCALM) at the University of Florida. This research was funded by NSF grant EAR-0207365, NCALM, the Southern California Earthquake Center (SCEC), the University of California, Lawrence Livermore National Laboratory UEPP program, a NASA Earth System Science Fellowship, the Geological Society of America, Sigma Xi, and the USC Department of Earth Sciences. SCEC is funded by NSF Cooperative Agreement EAR-0106924 and USGS Cooperative Agreement 02HQAG0008. This is SCEC contribution 958. This study was performed under the auspices of the U.S. Department of Energy by the University of California Lawrence Livermore National Laboratory, contract B539647. Gilles Peltzer, Lucilla Benedetti, and Isabelle Manighetti provided reviews that helped improve the manuscript.

References

Anderson, R. S., J. L. Repka, and G. S. Dick (1996), Explicit treatment of inheritance in dating depositional surfaces using in situ ^{10}Be and ^{26}Al, *Geology*, *24*, 47–51.

Argus, D. F., and R. G. Gordon (2001), Present tectonic motion across the Coast Ranges and San Andreas fault system in central California, *Geol. Soc. Am. Bull.*, *113*, 1580–1592.

Bartley, J. M., A. F. Glazner, and E. R. Schermer (1990), North-south contraction of the Mojave block and strike-slip tectonics in southern California, *Science*, *248*, 1398–1401.

Beanland, S., and M. M. Clark (1994), The Owens Valley fault zone, eastern California, and surface faulting associated with the 1872 earthquake, *U.S. Geol. Surv. Bull.*, *1982*, 29 pp.

Belmont, P., F. J. Pazzaglia, and J. Gosse (2006), Using the ^{10}Be grain size dependency in alluvial sediments to investigate hillslope and channel processes, *Eos Trans. AGU*, *87*(52), Fall Meet. Suppl., Abstract H21H-06.

Bennett, R. A., B. P. Wernicke, J. L. Davis, P. Elosegui, J. K. Snow, M. Abolins, M. A. House, G. L. Stirewalt, and D. A. Ferrill (1997), Global Positioning System constraints on fault slip rates in the Death Valley region, California and Nevada, *Geophys. Res. Lett.*, *24*, 3073–3076.

Bennett, R. A., B. P. Wernicke, N. A. Niemi, A. M. Friedrich, and J. L. Davis (2003), Contemporary strain rates in the northern Basin and Range province from GPS data, *Tectonics*, *22*(2), 1008, doi:10.1029/2001TC001355.

Bennett, R. A., A. M. Friedrich, and K. P. Furlong (2004), Codependent histories of the San Andreas and San Jacinto fault zones from inversion of fault displacement rates, *Geology*, *32*, 961–964.

Bevington, P. R., and D. K. Robinson (2003), *Data Reduction and Error Analysis for the Physical Sciences*, 320 pp., McGraw-Hill, New York.

Bierman, P. R., A. R. Gillespie, and M. W. Caffee (1995), Cosmogenic ages for earthquake recurrence intervals and debris flow fan deposition, Owens Valley, California, *Science*, *270*, 447–450.

Birkeland, P. W. (1999), *Soils and Geomorphology*, 372 pp., Oxford Univ. Press, New York.

Brogan, G. E., K. S. Kellog, D. B. Slemmons, and C. L. Terhune (1991), Late Quaternary faulting along the Death-Valley Furnace Creek fault system, California and Nevada, *U.S. Geol. Surv. Bull.*, *1991*, 23 pp.

Brown, E. T., R. F. Stallard, M. C. Larsen, D. L. Bourles, G. M. Raisbeck, and F. Yiou (1998), Determination of predevelopment denudation rates of an agricultural watershed (Cayaguas River, Puerto Rico) using in-situ-produced ^{10}Be in river-borne quartz, *Earth Planet. Sci. Lett.*, *160*, 723–728.

Bull, W. B. (1972), Recognition of alluvial fan deposits in the stratigraphic record, in *Recognition of Ancient Sedimentary Environments*, edited by J. K. Rigby and W. K. Hamblin, *Special Publ. SEPM Soc. Sediment. Geol.*, *16*, 63-83.

Bull, W. B. (1991), *Geomorphic Responses to Climatic Change*, 326 pp., Oxford Univ. Press, New York.

Carter, W., R. Shrestha, G. Tuell, D. Bloomquist, and M. Sartori (2001), Airborne laser swath mapping shines new light on Earth's topography, *Eos Trans. AGU*, *82*, 549, 550, 555.

Carter, B., R. L. Shrestha, and B. Dietrich (2003), National center for airborne laser mapping proposed, *Eos Trans. AGU*, *84*, 281, 285.

Cartwright, J. A., and C. S. Mansfield (1998), Lateral displacement variation and lateral tip geometry of normal faults in the Canyonlands National Park, Utah, *J. Struct. Geol.*, *20*, 3–19.

Clapp, E. M., P. R. Bierman, A. P. Schick, J. Lekach, Y. Enzel, and M. Caffee (2000), Sediment yield exceeds sediment production in arid region drainage basins, *Geology*, *28*, 995–998.

Clapp, E. M., P. R. Bierman, and M. Caffee (2002), Using ^{10}Be and ^{26}Al to determine sediment generation rates and identify sediment source areas in arid region drainage basins, *Geomorphology*, *45*, 89–104.

Dixon, T. H., S. Robaudo, J. Lee, and M. C. Reheis (1995), Constraints on present-day Basin and Range deformation from space geodesy, *Tectonics*, *14*, 755–772.

Dixon, T. H., M. Miller, F. Farina, H. Wang, and D. Johnson (2000), Present-day motion of the Sierra Nevada block and some tectonic implications for the basin and Range province, North American Cordillera, *Tectonics*, *19*, 1–24.

Dixon, T. H., E. Norabuena, and L. Hotaling (2003), Paleoseismology and global positioning system: Earthquake-cycle effects and geodetic versus geologic fault slip rates in the eastern California shear zone, *Geology*, *31*, 55–58.

Dokka, R. K., and C. J. Travis (1990), Late Cenozoic strike-slip faulting in the Mojave Desert, California, *Tectonics*, *9*, 311–340.

Dolan, J. F., D. D. Bowman, and C. G. Sammis (2007), Long-range and long-term fault interactions in southern California, *Geology*, in press.

Du, Y., and A. Aydin (1996), Is the San Andreas big bend responsible for the Landers earthquake and the eastern California shear zone?, *Geology*, *24*, 219–222.

Ellis, M. A., and W. J. Dunlap (1988), Displacement variation along thrust faults: Implications for the development of large faults, *J. Struct. Geol.*, *10*, 183–192.

Elmore, D., and F. M. Phillips (1987), Accelerator mass spectrometry for measurement of long-lived radioisotopes, *Science*, *236*, 543–550.

Elmore, D., B. R. Fulton, M. R. Clover, J. R. Marsden, H. E. Gove, H. Naylor, K. H. Purser, L. R. Kilius, R. P. Beukens, and A. E. Litherland (1979), Analysis of ^{36}Cl in environmental water samples using an electrostatic accelerator, *Nature*, *277*, 22–25.

Finkel, R. C., and M. Suter (1993), AMS in the earth sciences: Techniques and applications, *Adv. Anal. Geochem.*, *1*, 1–114.

Frankel, K. L., and J. F. Dolan (2007), Characterizing arid-region alluvial fan surface roughness with airborne laser swath mapping data, *J. Geophys. Res.*, *112*, F02025, doi:10.1029/2006JF000644.

Frankel, K. L., J. S. Pigati, J. S. Hoeft, N. F. Lifton, and J. F. Dolan (2004), Drainage basin erosion rates along the Death Valley fault zone, California from in-situ cosmogenic ^{14}C in alluvial sediment: Preliminary results, *Eos Trans. AGU*, *85*(47), Fall Meet. Suppl., Abstract H51C-1143.

Friedrich, A. M., B. P. Wernicke, N. A. Niemi, R. A. Bennett, and J. L. Davis (2003), Comparison of geodetic and geologic data from the Wasatch region, Utah, and implications for the spectral character of Earth deformation at periods of 10 to 10 million years, *J. Geophys. Res.*, *108*(B4), 2199, doi:10.1029/2001JB000682.

Friedrich, A. M., J. Lee, B. P. Wernicke, and K. Sieh (2004), Geologic context of geodetic data across a Basin and Range normal fault, Crescent Valley, Nevada, *Tectonics*, *23*, TC2015, doi:10.1029/2003TC001528.

Gan, W., J. L. Svarc, J. C. Savage, and W. H. Prescott (2000), Strain accumulation across the eastern California shear zone at latitude 36°30′N, *J. Geophys. Res.*, *105*, 16,229–16,236.

Gosse, J. C., and F. M. Phillips (2001), Terrestrial in situ cosmogenic nuclides: theory and application, *Quat. Sci. Rev.*, *20*, 1475–1560.

Guest, B., N. Niemi, and B. Wernicke (2005), A measure of post-mid-Miocene offset on the Stateline fault, California and Nevada, *Geol. Soc. Am. Abstr. Programs*, 36, Abstract 122-13.

Hancock, G. S., R. S. Anderson, O. A. Chadwick, and R. C. Finkel (1999), Dating fluvial terraces with ^{10}Be and ^{26}Al profiles: Application to the Wind River, Wyoming, *Geomorphology*, *27*, 41–60.

Harvey, A. M. (1997), The role of alluvial fans in arid zone fluvial systems, in *Arid Zone Geomorphology: Processes, Form and Change in Drylands*, edited by D. S. G. Thomas, 231-259, John Wiley, Hoboken, N. J.

Humphreys, E. D., and R. J. Weldon (1994), Deformation across the western United States: A local estimate of Pacific-North America transform deformation, *J. Geophys. Res.*, *99*, 19,975–20,010.

Jayko, A. S. (2005), Late Quaternary denudation, Death and Panamint valleys, eastern California, *Earth Sci. Rev.*, *73*, 271–289.

Klinger, R. E. (2001), Stop A3: Evidence for large dextral offset near Red Wall Canyon, in *Quaternary and Late Pliocene Geology of the Death Valley Region: Recent Observations on Tectonic, Stratigraphy, and Lake Cycles*, edited by M. N. Machette, M. L. Johnson, and J. L. Slate, *U.S. Geol. Surv. Open File Rep., 01-51*, A32-A37.

Klinger, R. E. (2002), Quaternary stratigraphy and geomorphology of northern Death Valley - Implications for tectonic activity along the northern Death Valley fault, Ph.D. dissertation, 312 pp., Univ. of Colo., Boulder.

Knott, J. R., J. C. Tinsley III, and S. G. Wells (2002), Are the benches at Mormon Point, Death Valley, California, USA, scarps or shorelines?, *Quat. Res.*, *58*, 352–360.

Kohl, C. P., and K. Nishiizumi (1992), Chemical isolation of quartz for measurement of in-situ-produced cosmogenic nuclides, *Geochim. Cosmochim. Acta*, *56*, 3583–3587.

Ku, T. L., S. Luo, T. K. Lowenstein, J. Li, and R. J. Spencer (1998), U-series chronology of lacustrine deposits in Death Valley, California, *Quat. Res.*, *50*, 261–275.

Lal, D. (1987), Cosmogenic nuclides produced in situ in terrestrial solids, *Nucl. Instrum. Methods Phys. Res., Ser. B*, *29*, 238–245.

Lal, D. (1991), Cosmic ray labeling of erosion surfaces: In situ production rates and erosion models, *Earth Planet. Sci. Lett.*, *104*, 424–439.

Lee, J., and D. Stockli (2006), (U-Th)/He apatite age data from the Inyo Mountains, California: Implications for the timing of extension and dextral slip rates along the western boundary of the Basin and Range province/eastern California shear zone, *Eos Trans. AGU*, *87*(52), Fall Meet. Suppl., Abstract T31B-0445.

Lee, J., C. M. Rubin, and A. Calvert (2001a), Quaternary faulting history along the Deep Springs fault, California, *Geol. Soc. Am. Bull.*, *113*, 855–869.

Lee, J., J. Q. Spencer, and L. A. Lowen (2001b), Holocene slip rates along the Owens Valley fault, California: Implications for the recent evolution of the eastern California shear zone, *Geology*, *29*, 819–822.

Li, Q., and M. Liu (2006), Geometrical impact of the San Andreas Fault on stress and seismicity in California, *Geophys. Res. Lett.*, *33*, L08302, doi:10.1029/2005GL025661.

Lubetkin, L., and M. M. Clark (1988), Late Quaternary activity along the Lone Pine fault, eastern California, *Geol. Soc. Am. Bull.*, *79*, 509–512.

Ludwig, K. R. (2003), Isoplot 3.00: A geochronological toolkit for Microsoft Excel, 71 pp., *Berkeley Geochronol. Center Spec. Publ.*, *4*.

Machette, M. N., C. N. Martinez, A. J. Crone, K. M. Haller, and G. D'Addezio (1999), Geological and seismic hazard investigations of the Cow Creek area, Death Valley National Park, California, *U.S. Geol. Surv. Open File Rep.*, *99-0155*, 42 pp.

Machette, M. N., R. E. Klinger, J. R. Knott, C. J. Wills, W. A. Bryant, and M. C. Reheis (2001), A proposed nomenclature for the Death Valley fault system, in *Quaternary and Late Pliocene Geology of the Death Valley Region: Recent Observations on Tectonic, Stratigraphy, and Lake Cycles*, edited by M. N. Machette, M. L. Johnson, and J. L. Slate, *U.S. Geol. Surv. Open File Rep., 01-51*, J173-J183.

Maerten, L., E. J. M. Willemse, D. D. Pollard, and K. Rawnsley (1999), Slip distributions on intersecting normal faults, *J. Struct. Geol.*, *21*, 259–271.

Manighetti, I., G. C. P. King, Y. Gaudemer, C. H. Scholz, and C. Doubre (2001), Slip accumulation and lateral propagation of active normal faults in Afar, *J. Geophys. Res.*, *106*, 13,667–13,696.

Manighetti, I., M. Campillo, C. Sammis, P. M. Mai, and G. King (2005), Evidence for self-similar, triangular slip distributions on earthquakes: Implications for earthquake and fault mechanics, *J. Geophys. Res.*, *110*, B05302, doi:10.1029/2004JB003174.

Matmon, A., P. R. Bierman, J. Larsen, S. Southworth, M. Pavich, R. Finkel, and M. Caffee (2003), Erosion of an ancient mountain range, the Great Smoky Mountains, North Carolina and Tennessee, *Am. J. Sci.*, *303*, 817–855.

Matmon, A., D. P. Schwartz, R. Finkel, S. Clemmens, and T. Hanks (2005), Dating offset fans along the Mojave section of the San Andreas fault using cosmogenic ^{26}Al and ^{10}Be, *Geol. Soc. Am. Bull.*, *117*, 795–807, doi:10.1130/B25590.1.

Matmon, A., K. Nichols, and R. Finkel (2006), Isotopic insights into smoothening of abandoned fan surfaces, southern California, *Quat. Res.*, *66*, 109–118.

McClusky, S. C., S. C. Bjornstad, B. H. Hager, R. W. King, B. J. Meade, M. M. Miller, F. C. Monastero, and B. J. Souter (2001), Present day kinematics of the eastern California shear zone from a geodetically constrained block model, *Geophys. Res. Lett.*, *28*, 3369–3372.

Miller, M. M., D. J. Johnson, T. H. Dixon, and R. K. Dokka (2001), Refined kinematics of the eastern California shear zone from GPS observations, 1993–1994, *J. Geophys. Res.*, *106*, 2245–2263.

Niemi, N. A., B. P. Wernicke, R. J. Brady, J. B. Saleeby, and G. C. Dunne (2001), Distribution and provenance of the middle Miocene Eagle Mountain Formation, and implications for regional kinematic analysis of the Basin and Range province, *Geol. Soc. Am. Bull.*, *113*, 419–442.

Nur, A., H. Ron, and G. C. Beroza (1993), The nature of the Landers-Mojave earthquake line, *Science*, *261*, 201–203.

Oskin, M., and A. Iriondo (2004), Large magnitude transient strain accumulation on the Blackwater fault, eastern California shear zone, *Geology*, *32*, 313–316.

Oskin, M., L. Perg, E. Shelef, M. Strane, E. Gurney, D. Blummentritt, A. Iriondo, S. Mukhopadhyay, and B. Singer (2006), Geologic fault slip rates support transitory, elevated geodetic strain accumulation across the Mojave Desert, eastern California shear zone, *Eos Trans. AGU*, *87*(52), Fall Meet. Suppl., Abstract G43B-0992.

Oskin, M., L. Perg, D. Blumentritt, S. Mukhopadhyay, and A. Iriondo (2007), Slip rate of the Calico fault: Implications for geologic versus geodetic rate discrepancy in the eastern California shear zone, *J. Geophys. Res.*, *112*, B03402, doi:10.1029/2006JB004451.

Oswald, J. A., and S. G. Wesnousky (2002), Neotectonics and Quaternary geology of the Hunter Mountain fault zone and Saline Valley region, southeastern California, *Geomorphology*, *42*, 255–278.

Peacock, D. C. P., and D. J. Sanderson (1991), Displacements, segment linkage and relay ramps in normal fault zones, *J. Struct. Geol.*, *13*, 721–733.

Peltzer, G., F. Crampe, S. Hensley, and P. Rosen (2001), Transient strain accumulation and fault interaction in the eastern California shear zone, *Geology*, *29*, 975–978.

Phillips, F. M., and M. A. Plummer (1996), CHLOE: A program for interpreting in-situ cosmogenic nuclide data for surface exposure dating and erosion studies, *Radiocarbon*, *38*, 98–99.

Phillips, F. M., B. D. Leavy, N. D. Jannik, D. Elmore, P. W. Kubik, R. I. Dorn, and D. J. Roddy (1986), The accumulation of cosmogenic chlorine-36 in rocks: A method for surface exposure dating, *Science*, *231*, 41–43.

Phillips, F. M., W. D. Stone, and J. T. Fabryka-Martin (2001), An improved approach to calculating low-energy cosmic-ray neutron fluxes near the land/atmosphere interface, *Chem. Geol.*, *175*, 689–701.

Phillips, F. M., J. P. Ayarbe, B. J. Harrison, and D. Elmore (2003), Dating rupture events on alluvial fault scarps using cosmogenic nuclides and scarp morphology, *Earth Planet. Sci. Lett.*, *215*, 203–218.

Pollitz, F. F., and I. S. Sacks (1992), Modeling of postseismic relaxation following the great 1857 earthquake, southern California, *Seismol. Soc. Am. Bull.*, *82*, 454–480.

Reheis, M. C., and T. H. Dixon (1996), Kinematics of the eastern California shear zone: Evidence for slip transfer from Owens and Saline Valley fault zones to Fish Lake Valley fault zone, *Geology*, *24*, 339–342.

Reheis, M. C., and T. L. Sawyer (1997), Late Cenozoic history and slip rates of the Fish Lake Valley, Emigrant Peak, and Deep Springs fault zones, Nevada and California, *Geol. Soc. Am. Bull.*, *109*, 280–299.

Reid, I., and L. E. Frostick (1997), Channel form, flows and sediments in deserts, in *Arid Zone Geomorphology: Processes, Form and Change in Drylands*, edited by D. S. G. Thomas, 205-229, John Wiley, Hoboken, N. J.

Repka, J. L., R. S. Anderson, and R. C. Finkel (1997), Cosmogenic dating of fluvial terraces, Fremont River, Utah, *Earth Planet. Sci. Lett.*, *152*, 59–73.

Reynolds, M. W. (1969), Stratigraphy and structural geology of the Titus and Titanothere Canyons area, Death Valley, California, Ph.D. dissertation, 310 pp., Univ. of Calif., Berkeley.

Rockwell, T. K., S. Lindvall, M. Herzberg, D. Murbach, T. Dawson, and G. Berger (2000), Paleoseismology of the Johnson Valley, Kickapoo, and Homestead Valley faults: Clustering of earthquakes in the eastern California shear zone, *Bull. Seismol. Soc. Am.*, *90*, 1200–1236.

Sartori, M. (2005), ALSM acquisition in Death Valley National Park, Report on Data Processing, 13 pp., Natl. Center for Airborne Laser Mapp., Univ. of Fla., Gainesville.

Savage, J. C., and M. Lisowski (1995), Strain accumulation in Owens Valley, California, *Bull. Seismol. Soc. Am.*, *85*, 151–158.

Savage, J. C., M. Lisowski, and W. H. Prescott (1990), An apparent shear zone trending north-northwest across the Mojave Desert into Owens Valley, *Geophys. Res. Lett.*, *17*, 2113–2116.

Schweickert, R. A., and M. M. Lahren (1997), Strike-slip fault system in Armagosa Valley and Yucca Mountain, Nevada, *Tectonophysics*, *272*, 25–41.

Sella, G. F., T. H. Dixon, and A. Mao (2002), REVEL: A model for Recent plate velocities from space geodesy, *J. Geophys. Res.*, *107*(B4), 2081, doi:10.1029/2000JB000033.

Sieh, K. E., and R. H. Jahns (1984), Holocene activity of the San Andreas fault at Wallace Creek, California, *Geol. Soc. Am. Bull.*, *95*, 883–896.

Snow, J. K., and B. P. Wernicke (1989), Uniqueness of geological correlations: An example from the Death Valley extended terrain, *Geol. Soc. Am. Bull.*, *101*, 1351–1362.

Stone, J. O. (2000), Air pressure and cosmogenic isotope production, *J. Geophys. Res.*, *105*, 23,753–23,759.

Stone, J., J. Evans, K. Fifield, R. Cresswell, and G. Allan (1996a), Cosmogenic chlorine-36 production rates from calcium and potassium, *Radiocarbon*, *38*, 170–171.

Stone, J. O., G. L. Allan, L. K. Fifield, and R. G. Cresswell (1996b), Cosmogenic chlorine-36 from calcium spallation, *Geochim. Cosmochim. Acta*, *60*, 679–692.

Stone, J. O. H., J. M. Evans, L. K. Fifield, G. L. Allan, and R. G. Cresswell (1998), Cosmogenic chlorine-36 production in calcite by muons, *Geochim. Cosmochim. Acta*, *62*, 433–454.

Tarboton, D. G., R. L. Bras, and I. Rodriguez-Iturbe (1991), On the extraction of channel networks from digital elevation data, *Hydrol. Processes*, *5*, 81–100.

van der Woerd, J., P. Tapponier, F. J. Ryerson, A. S. Meriaux, B. Meyer, Y. Gaudemer, R. C. Finkel, M. W. Caffee, G. Zhao, and Z. Xu (2002), Uniform postglacial slip-rate along the central 600 km of the Kunlun fault (Tibet), from ^{26}Al, ^{10}Be, and ^{14}C dating of riser offsets, and climatic origin of the regional morphology, *Geophys. J. Int.*, *148*, 356–388.

van der Woerd, J., Y. Klinger, K. Sieh, P. Tapponnier, F. J. Ryerson, and A.-S. Mériaux (2006), Long-term slip rate of the southern San Andreas fault from ^{10}Be-^{26}Al surface exposure dating of an offset alluvial fan, *J. Geophys. Res.*, *111*, B04407, doi:10.1029/2004JB003559.

Weldon, R., K. Scharer, T. Fumal, and G. Biasi (2004), Wrightwood and the earthquake cycle: What a long recurrence record tells us about how faults work, *GSA Today*, *14*, 4–10.

Wernicke, B., A. M. Friedrich, N. A. Niemi, R. A. Bennett, and J. L. Davis (2000), Dynamics of plate boundary fault systems from Basin and Range Geodetic Network (BARGEN) and geologic data, *GSA Today*, *10*, 1–7.

Wernicke, B., J. L. Davis, R. A. Bennett, J. E. Normandeau, A. M. Friedrich, and N. A. Niemi (2004), Tectonic implications of a dense continuous GPS velocity field at Yucca Mountain, Nevada, *J. Geophys. Res.*, *109*, B12404, doi:10.1029/2003JB002832.

Wernicke, B., N. Niemi, J. L. Davis, S. Bisnath, and P. Elosegui (2005), Tectonic megaoscillators: Implications for large-scale stress transfer in the lithosphere, *Geol. Soc. Am. Abstr. Programs*, *36*, Abstract 55-13.

Wesnousky, S. G. (1988), Seismological and structural evolution of strike-slip faults, *Nature*, *335*, 340–343.

Zreda, M. G. (1994), Development and calibration of the cosmogenic ^{36}Cl surface exposure dating method and its applications to the chronology of late Quaternary glaciations, Ph.D. thesis, 318 pp., N. M. Inst. of Min. and Technol., Socorro.

K. S. Brantley and B. P. Wernicke, Division of Geological and Planetary Sciences, California Institute of Technology, Pasadena, CA 91125, USA. (kathy@alumni.caltech.edu; brian@gps.caltech.edu)

R. C. Finkel, Center for Accelerator Mass Spectrometry, Lawrence Livermore National Laboratory, Livermore, CA 94550, USA. (finkel1@llnl.gov)

K. L. Frankel and J. F. Dolan, Department of Earth Sciences, University of Southern California, Los Angeles, CA 90089, USA. (kfrankel@usc.edu; dolan@usc.edu)

R. E. Klinger, Technical Service Center, U.S. Bureau of Reclamation, P.O. Box 25007, D-8330, Denver, CO 80225, USA. (rklinger@do.usbr.gov)

J. R. Knott, Department of Geological Sciences, California State University, Fullerton, CA 92831, USA. (jknott@fullerton.edu)

M. N. Machette and J. L. Slate, Central Region Geologic Hazards Team, U.S. Geological Survey, Lakewood, CO 80225, USA. (machette@usgs.gov; jslate@usgs.gov)

L. A. Owen, Department of Geology, University of Cincinnati, Cincinnati, OH 45221, USA. (lewis.owen@uc.edu)

F. M. Phillips, Department of Earth and Environmental Science, New Mexico Institute of Mining and Technology, Socorro, NM 87801, USA. (phillips@nmt.edu)